10

Stereology

10.1 Introduction

The objective of stereology is to draw inferences about the geometrical properties of three-dimensional structures when information is only available in lower-dimensional form via planar sections, linear probes, or projections of thick slices. Its application arises in the study of geometrical structure of constituents in opaque or partially opaque bodies such as metals, minerals, synthetic materials, food or biological tissues. Often these structures appear at the microscale, but sometimes also the macroscale is of interest, for example in studies of rock or soil structures. In all these cases an elegant way to acquire spatial information is via planar sections or linear probes.

Fortunately, today there exist various techniques that yield spatial information in a direct way, for example computerised tomography (CT) based on absorption of X-rays or synchrotron radiation and reconstruction of three-dimensional (3D) data from stacks of two-dimensional (2D) images obtained by confocal laser scanning microscopy. In the first case the inverse Radon transform is applied, in the second methods of differential calculus. Furthermore, 3D images can be obtained by serial sections combined with classical microscopic imaging such as focused ion beam thinning combined with scanning electron microscopy. The data obtained can be analysed with the methods described, for example, in Chapter 6. The 3D-data-yielding methods can be seen as using many sections close together, while in stereology as understood in this chapter the number of sections is small and these are placed in large distances such that the measurement results can be considered as independent.

Some stereological methods that were too complicated and instable are now obsolete. However, there are many very simple and elegant stereological techniques which make the use of 3D techniques unnecessary, as for example, the methods for determining the so-called 'global parameters' (Rhines, 1986) such as volume fraction V_V, specific surface area S_V and specific line length L_V; see the discussion in Exner (2004). Additionally, planar sections are sometimes observable 'with much higher precision than is available in 3D and hence the only way to gain information about the 3D objects is to study 2D sections of them', in particular if

Stochastic Geometry and its Applications, Third Edition.
Sung Nok Chiu, Dietrich Stoyan, Wilfrid S. Kendall and Joseph Mecke.

one is interested in nano-scale objects (Nagel, 2010). The wording in Torquato (2002, p. 294) describing stereology as a 'poor man's' tomography or in Baddeley and Jensen (2005, p. 81) as 'cheap technique' should not be considered ruling out the use of stereology. Stereology should be applied when other techniques are too expensive or cannot be successfully applied. (Wise rich men use their resources economically.)

Traditionally, stereology represents an important part of the applications of stochastic geometry and spatial statistics. This chapter introduces many of the results and ideas of stereology, limited mainly to cases where statistically homogeneous structures are of interest. Such applications are typical in materials science, geological science and food science (Baddeley and Jensen, 2005) and in some cases in medicine or biology. There are various textbooks on the topic starting with the classical books by Underwood (1970) and Saltykov (1974), namely Weibel (1980), Saxl (1989), Ohser and Mücklich (2000), Hilliard and Lawson (2003), Baddeley and Jensen (2005), Howard and Reed (2005) and Mouton (2011). And the fine survey of Nagel (2010) written for mathematicians has to be mentioned.

The methods and formulae of stereology relate characteristics of three-dimensional structures to quantities arising from measurements of planar sections (such as slices through metallic or mineral material), projections of thick sections (such as foils or sheets of biological material studied by light or electron microscopy), or linear probes (such as arising in biopsy or geological drilling).

The step from spatial structures to planar or linear sections or from planar structures to linear probes involves much loss of information and so stereological methods commonly can yield only 'global' information of a statistical character. A further consequence of this loss of information is that some of the applications require the solution of *ill-posed* mathematical problems, that is, numerical problems in which small deviations of data (perhaps due to measurement errors and statistical fluctuations) can lead to large discrepancies in the final solution. For example, this is the case for the Wicksell corpuscle problem, the unfolding problem for ball diameters in Section 10.4.

Stereological formulae depend on some assumption of 'randomness'. This can come in one of two forms: either the structure itself is assumed to be random or the section process is taken to involve a randomising element. In the first case stereologists speak about the

model-based approach

and in the second case about the

design-based approach.

For scientists using stereology in materials science and technology, mineralogy, geology, and food science it is usually natural to follow the model-based approach and to assume that the structures are motion-invariant, that is, stationary (statistically homogeneous) and isotropic. In many cases motion-invariance is the only mathematical assumption, and it alone already leads to valuable results. (However, finer model assumptions such as that the observed structure is a system of balls are often of interest and hence are also discussed as special cases.) In the mathematical theory it is then possible to assume that the section plane or line is fixed, for example the section plane is taken to be the (x_1, x_2)-plane. This book mainly follows the model-based approach. The alternative approach typically assumes that the sectioning planes or lines are members of motion-invariant plane or line processes, which is more natural in biological applications. The design-based approach is described in detail in the book by Baddeley and

Jensen (2005). A reader of that book may read the term 'modern stereology' as 'modern biological stereology'. In actual practice, many stereological formulae are generally similar for both approaches, differing only in the statistical theory and underlying interpretation; see Jensen (1984), Stoyan (1990b) and Baddeley and Jensen (2005).

A special instance of design-based techniques is the area of *local stereology*. 'The target is here quantitative parameters of structures which can be regarded as neighbourhoods of points, called reference points. An important example is the case where the structure is a biological cell and the reference point is the cell nucleus or some identifiable part of the nucleus such as the nucleolus' (Jensen, 1998, p. 27). Inferences are drawn using random lines or planes through the reference point, based on physical or optical sections. The Horvitz–Thompson estimator plays an important rôle.

Design-based stereology as in Baddeley and Jensen (2005) is substantially based on ideas of sampling theory and opens the way to characterise the precision of stereological estimators. It applies various random sampling designs which are adapted to the case of inhomogeneous or even finite structures.

Historically, Delesse (1847) and Rosiwal (1898) are landmark papers in the development of stereology, recognising that under certain conditions the volume fraction of a component in a body equals the area or linear fraction in planar or linear section; see Sections 6.4.2 and 10.2.2. Wicksell (1925) solved the problem of inferring the size distribution for systems of balls given planar sections; see Section 10.4.2. Beginning with the 1940s the stereological theory has been developed by researchers such as Bach, Cruz-Orive, DeHoff, Giger, Hilliard, Moran, and Saltykov. The mathematical basis of modern stereology is due to Ambartzumian, Baddeley, Coleman, Cruz-Orive, Davy, Gundersen, Jensen, Miles, Saxl and others, with important impulses for its development coming repeatedly from the needs of practical applications. The modern mathematical–statistical theory is a synthesis of integral geometry, stochastic geometry and sampling theory. For example, the proof on p. 428 demonstrates the use of point processes; random measure theory occurs in Section 8.3 in the proofs of section-formulae for fibre processes.

10.2 The fundamental mean-value formulae of stereology

10.2.1 Notation

Stereology is built on a small number of mean-value formulae concerning intensities of random measures, which belong to the *global parameters*. These quantities, often also called *densities* or *specific values*, arise here as intensities of stationary (often isotropic) random measures. These are listed systematically in Table 10.1, using a system described originally in Underwood (1976) and Weibel (1980). It is used throughout this book and is here explained systematically.

Each mean-value quantity is denoted by one symbol subscripted by another. The main symbol is the quantity measured while the subscripted symbol indicates the dimensionality of the section employed in the measurement.

For example, the symbol A_A denotes the mean area of some constituent of the structure being considered per unit area. It is therefore the *area density* or *area fraction* of the constituent. The notation S_V stands for the mean surface area per unit volume, the *surface density* or *specific surface (area)*; it is measured in units of $\mathrm{m}^2/\mathrm{m}^3$.

In the following, Ξ_V is the 3D constituent of interest and Ξ_A its planar section.

Table 10.1 Symbols in common use in stereology.

	Interpretation of main symbol
V	Volume (in m^3)
S	Surface area (in m^2)
M	Integral of mean curvature (in m)
A	Planar area (of profiles or section structures) (in m^2)
L	Length (of linear elements in the space or plane) (in m)
N	Number of grains, particles or section profiles (for non-overlapping germ–grain models) or more generally the connectivity number
P	Number of points (in a section)
	Interpretation of symbol in subscript
V	per unit volume
A	per unit area
L	per unit length
P	per point

10.2.2 Planar and linear sections

The following presents the general stereological formulae that arise when the structure is sectioned by a plane or line; see Figure 10.1. Each formula will be stated and followed by either a brief indication of its proof or a reference.

Volume fraction

The most important stereological formula is very simple. The volume fraction V_V of a stationary structure satisfies

$$V_V = A_A = L_L = P_P. \tag{10.1}$$

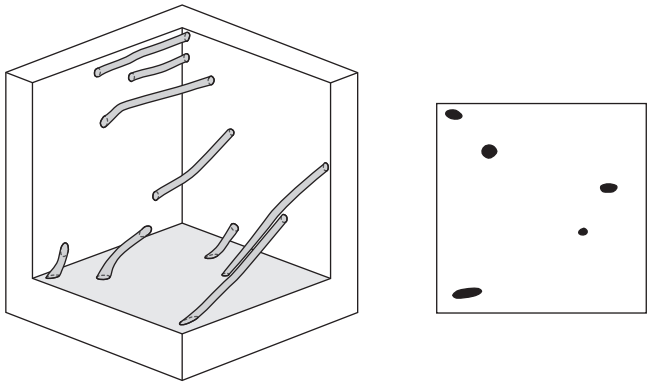

Figure 10.1 (a) A three-dimensional sample of fibres and (b) a planar section. The figure is based on a CT image kindly provided by Fraunhofer ITWM, showing a concrete sample with steel fibres obtained from the civil engineering department of TU Kaiserslautern.

That means, V_V can be obtained by planar or linear sections, or by measurement with a point lattice — without any assumption of isotropy. In mathematical terminology, the 'structure' is a stationary random set. The section plane or line can be arbitrary, but must be independent of the structure.

Equation-chain (10.1) can be interpreted as follows. The volume fraction V_V is equal to the quantity obtained by intersecting Ξ_V by an arbitrary test plane, line, or point system and measuring respectively the area fraction A_A, linear fraction L_L, or fraction P_P of test points in Ξ_V, respectively. Section 6.4.2 considers this further and discusses the estimation of A_A (or p in the notation there).

For example, let Ξ_A be the planar random closed set resulting from intersection of the stationary Ξ_V with a test plane, which is considered as the (x_1, x_2)-plane. Then Ξ_A is also stationary and so,

$$\begin{aligned} A_A &= \mathbf{E}\big(\nu_2(\Xi_A \cap [0,1]^2)\big) \\ &= \int_{[0,1]^2} \mathbf{P}(x \in \Xi_A)\,\mathrm{d}x = \mathbf{P}(o \in \Xi_A) = \mathbf{P}(o \in \Xi_V) \\ &= p = V_V, \end{aligned}$$

as discussed in Section 6.3.1.

Specific surface area

For a *motion-invariant* surface process, typically the surface of a three-dimensional motion-invariant random closed set, the following formulae were found by Saltykov (1945):

$$S_V = \frac{4}{\pi} L_A, \tag{10.2}$$

and

$$S_V = 2P_L. \tag{10.3}$$

This means that S_V can be estimated from planar sections by measuring line lengths and determining the intensity L_A, or from linear sections by counting the points formed by intersection of the linear probe with the surface of interest and calculating the mean number of intersection points per unit length; see Section 8.5.1.

In the anisotropic case there also exist elegant stereological methods for the determination of S_V. The following two cases are of particular interest.

(a) The surface process of interest is the result of a *homogeneous deformation* of an originally motion-invariant structure. Such a deformation is a mapping

$$(x_1, x_2, x_3) \mapsto (\eta_1 x_1, \eta_2 x_2, \eta_3 x_3)$$

with

$$\eta_1 \eta_2 \eta_3 = 1,$$

that is, it is volume-conserving. Samples of rolled steel can be described in this way, where $\eta_1 \le \eta_2 \le \eta_3$ represent the amounts of working. In this case lineal analysis measurements in the directions of x_1-, x_2- and x_3-axes lead to S_V as follows.

One determines the mean number $P_L^{(i)}$ of intersections of a test line in the direction of x_i-axis with the surface process of interest per length unit and so obtains estimators for the η_i via

$$\eta_1 P_L^{(1)} = \eta_2 P_L^{(2)} = \eta_3 P_L^{(3)} \tag{10.4}$$

and

$$\eta_1^3 = \frac{P_L^{(2)} P_L^{(3)}}{(P_L^{(1)})^2}, \qquad \eta_2^3 = \frac{P_L^{(1)} P_L^{(3)}}{(P_L^{(2)})^2}, \qquad \eta_3^3 = \frac{P_L^{(1)} P_L^{(2)}}{(P_L^{(3)})^2}. \tag{10.5}$$

The specific surface area S_V satisfies

$$S_V = 4P_L^{(1)} \frac{S(\eta_1, \eta_2, \eta_3)}{\pi \eta_2 \eta_3}, \tag{10.6}$$

$$S_V = 4P_L^{(2)} \frac{S(\eta_1, \eta_2, \eta_3)}{\pi \eta_1 \eta_3}, \tag{10.7}$$

$$S_V = 4P_L^{(3)} \frac{S(\eta_1, \eta_2, \eta_3)}{\pi \eta_1 \eta_2}, \tag{10.8}$$

see Ohser and Mücklich (2000, p. 90), where $S(a, b, c)$ is the surface area of an ellipsoid of semiaxes a, b and c. They also present an algorithm for the estimation of S_V for given estimates of the $P_L^{(i)}$, $i = 1, 2, 3$. Furthermore, there is a well-documented example with drawn wire, where $\eta_1 < \eta_2 = \eta_3$; the x_1-direction is the drawing direction.

(b) The surface process of interest is stationary and, in addition, its distribution is invariant with respect to rotations about axes parallel to a given direction, in the following considered as the x_3-axis. (This x_3-rotation invariance corresponds to the equality $\eta_1 = \eta_2$ in case (a) above.) In this situation the specific surface area can be estimated from only one section plane, by *vertical section*.

A vertical plane is a plane parallel to the vertical axis. It yields a line of intersection with the (x_1, x_2)-plane, which uniquely determines the section plane.

The intersection of the vertical plane with the surface process yields a planar fibre process. This fibre process is intersected with a system of test curves as shown in Figure 10.2 and the number of fibre–curve intersection points is counted. The mean number P_L of intersection points per unit curve length leads, via Formula (10.3), to S_V. Note that the line density L_A of the fibre process in general does not satisfy Formula (10.2).

The curves in Figure 10.2 are so-called cycloids given by the parametric form

$$x_1 = \theta - \sin\theta \quad \text{and} \quad x_2 = 1 - \cos\theta$$

for $0 \le \theta \le \pi$. Such a curve has vertical height 2, horizontal width π and length 4. The tangent directions have the direction probability density function $f(\alpha) = \frac{1}{2}\sin\alpha$, which appears in Section 8.4.

Practical vertical S_V-measurement consists in taking n random vertical planes (constructed from random lines in the (x_1, x_2)-plane as in Section 8.2.2) and in using on each of them a

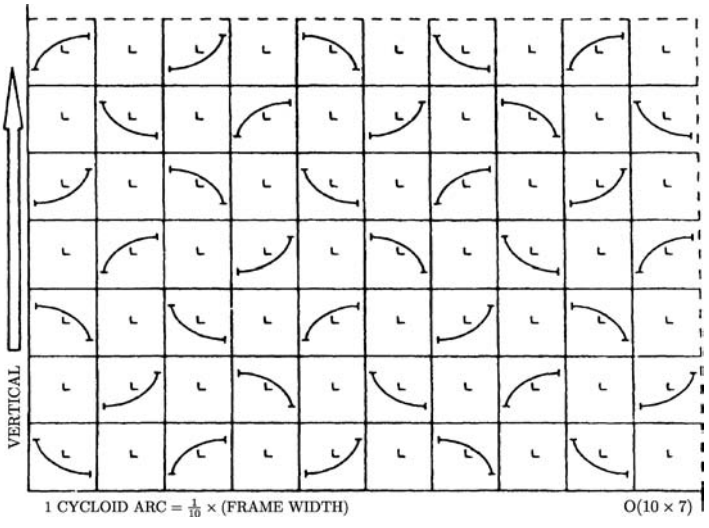

Figure 10.2 A test system of cycloids for estimating S_V from vertical sections. Reproduced from Baddeley *et al.* (1986) with permission of Wiley.

system of cycloids as shown in Figure 10.2. For the i^{th} plane, where the total length of all cycloids is l_i, the number P_i of intersection points of the surface process with the cycloids is determined, $i = 1, 2, \ldots, n$. The sum of the P_i divided by the sum of the total lengths l_i leads to the estimator

$$\hat{S}_V = 2 \sum_{i=1}^{n} P_i \Big/ \sum_{i=1}^{n} l_i. \tag{10.9}$$

This method was developed by Spektor (1950) and rediscovered by Hilliard (1967). In a very general context it is described and discussed in Baddeley and Jensen (2005, Section 8.1).

Specific curve length

For a stationary and isotropic fibre process the specific curve length satisfies the following relation found by Smith and Guttman (1953):

$$L_V = 2P_A. \tag{10.10}$$

This means that L_V can be determined from a planar section by counting the number of points formed by intersection of a plane with the fibre process. Remarks on the proof are to be found in Section 8.4.

Specific integral of mean curvature

For a stationary and isotropic surface process the specific integral of mean curvature or integral of mean curvature density M_V is defined as the intensity of the mean curvature measure

associated with the process; see Section 7.3.4. It satisfies

$$M_V = C_A, \tag{10.11}$$

where C_A denotes the density of curvature of fibres in the planar section. In the terminology of Section 7.3.4 it is the intensity of the planar curvature measure. Formulae (7.56) and (10.11) yield

$$M_V = 2\pi N_A. \tag{10.12}$$

In the case of non-overlapping grains this formula is due to Bodziony (1965), where N_A is the mean number of section profiles per area unit. In the general case N_A is the specific planar connectivity number as introduced on p. 294.

Functional summary characteristics

In the motion-invariant case there are some random-set functional summary characteristics that can be easily determined from planar sections. As shown in Section 6.3, they are of great value in exploratory analyses. These characteristics are:

- covariance $C(r)$,
- linear contact distribution function $H_l(r)$,
- chord length distribution function $L(r)$,
- discoidal contact distribution function $H_d(r)$,
- all characteristics related to the capacity functional $T_{\Xi_A}(K)$ for planar K.

By the way, the first three characteristics can be obtained even from linear probes.

Stereological reconstruction

A powerful but computation-intensive method is stereological reconstruction for constituents in random structures that can be modelled by motion-invariant random sets. This method is a particular application of the general reconstruction method described in Section 6.7. Here the data come from a section plane, which is in the following identified with the (x_1, x_2)-plane, as a black–white pixel set. This pattern is analysed with the statistical methods for planar random sets as in Section 6.4 to yield estimates of $V_V = A_A$, $C(r)$, $H_l(r)$ and $H_d(r)$. Then a three-dimensional random set is simulated in the 'positive half-space' $\mathbb{R}^3_+ = \{(x_1, x_2, x_3) : x_3 \geq 0\}$ with the reconstruction method described in Section 6.7. The energy function used is an expression like

$$E = \alpha_C \int_0^{R_C} \big(\hat{C}(r) - C^s(r)\big)^2 \mathrm{d}r + \alpha_l \int_0^{R_l} \big(\hat{H}_l(r) - H_l^s(r)\big)^2 \mathrm{d}r + \alpha_d \int_0^{R_d} \big(\hat{H}_d(r) - H_d^s(r)\big)^2 \mathrm{d}r \tag{10.13}$$

with suitable weight parameters α_C, α_l and α_d and upper limits R_C, R_l and R_d. The aim is to obtain a pixel structure in $\mathbb{R}^3_+$ whose characteristics are as close as possible (in the sense that E is minimised) to the estimated characteristics $\hat{V}_V$, $\hat{C}(r)$, $\hat{H}_l(r)$ and $\hat{H}_d(r)$ of the given pattern. In (10.13), $C^s(r)$, $H_l^s(r)$ and $H_d^s(r)$ are the corresponding characteristics of the

simulated structure. It is easy to guarantee that $V_V^s = \hat{V}_V$ in the simulated structure, but for the other characteristics only approximation is possible, usually with simulated annealing.

This simulation is carried out *conditionally*, that is, on the (x_1, x_2)-plane the data structure is fixed during the whole simulation. This implies that for points with small x_3-coordinates the colours of the pixels are similar to the values at their neighbours in the section plane.

The three-dimensional pixel structure obtained by this simulation can be statistically analysed by the methods for three-dimensional random sets as in Section 6.4, and this leads to estimated characteristics that usually cannot by obtained by planar sections, such as the spherical contact distribution function $H_s(r)$, connectivity parameters beginning with the specific Euler–Poincaré characteristic N_V, or information on permeability and percolation.

The two papers of Talukdar *et al.* (2002,b) present interesting applications of this method. In both cases the two-dimensional data, which come from a pack of glass balls and North Sea chalk respectively, result from electron microscopic images. It is remarkable that these authors could demonstrate that their method produced good results though they only worked with $C(r)$ and $H_l(r)$ or $L(r)$. However, in general, using only $C(r)$ and $H_l(r)$ would result in reconstructed structures having poor pore space connectivity; see for example Øren and Bakke (2002, 2003) and Čapek *et al.* (2009). Li *et al.* (2012) compares reconstructions of three-dimensional structures using different summary characteristics.

10.2.3 Thick sections

To understand what a thick section is, see Figure 10.3 on p.435. The random closed set Ξ_V under study is intersected by two parallel planes separated by a distance $t > 0$. For the sake of definiteness one of these planes is taken to be the (x_1, x_2)-plane. The 'slice' that is to be examined is the set

$$T^t = \{\boldsymbol{x} = (x_1, x_2, x_3) : 0 \le x_3 \le t\}$$

lying between these two planes. The experimental data are the planar image Ξ^t of the orthogonal projection of $\Xi_V \cap T^t$ onto the (x_1, x_2)-plane, which is again a random set. The projected thick section Ξ^t inherits the properties of stationarity and isotropy from Ξ_V.

Note that the term 'thin sections' is also often used in the literature. The term 'thick sections' makes the contrast to 'planar sections', which have no thickness, whilst the term 'thin' refers to the fact that the thickness of such a section is very small; both terms can be used for the same problem.

Application of the classical stereological Formulae (10.1) and (10.2) to the planar data $A_A(t)$ and $L_A(t)$ explained below would yield biased estimates of V_V and S_V. Therefore refined formulae are necessary.

Volume fraction and specific surface area of porous media

There seem to be no exact general formulae relating V_V and S_V to intensities that are measurable on Ξ^t. However, formulae are known for particular cases. Section 10.3.2 gives examples. In the motion-invariant case an approximate formula is given by

$$V_V \approx A_A(t) - \frac{tL_A(t)}{\pi}, \tag{10.14}$$

where $A_A(t)$ is the area fraction and $L_A(t)$ the mean boundary length per unit area of Ξ^t. This formula was given by Cahn and Nutting (1959) for systems of convex non-overlapping particles and then a heuristic argument based on the theories of random closed sets and surface processes was given for more general structures; see Stoyan (1984a).

An approximation of a similar nature for S_V is

$$S_V \approx \frac{4}{\pi} L_A(t) - 4tN_A(t), \tag{10.15}$$

where $N_A(t)$ is the specific number of section profiles; see Ohser and Mücklich (2000, p. 79)

An alternative to (10.14) is the formula

$$A_A(t) = 1 - (1 - V_V) \exp\left(-\frac{S_V t}{4(1 - V_V)}\right), \tag{10.16}$$

derived by Overby and Johnson (2005). For S_V the approximation formula (10.15) can be plugged in.

Note that with $t \to 0$ the classical stereological formulae are obtained.

Length density of fibre processes

Let now Ξ_V be a spatial motion-invariant fibre process. The fibre pieces between the two section planes are orthogonally projected and Ξ^t is a planar motion-invariant fibre process. The length density L_V of Ξ_V satisfies

$$L_V = \frac{4}{\pi t} L_A(t), \tag{10.17}$$

where $L_A(t)$ is the specific curve length of Ξ^t. Nagel (1983) gave a proof using the theory of fibre processes. Together with Formula (8.38) this yields

$$L_V = \frac{2}{t} P_L(t), \tag{10.18}$$

where $P_L(t)$ is the mean number of intersection points of the x_1-axis with the projected fibres in the slice. Note that here the limit $t \to 0$ does not make sense.

Formula (10.18) is the base of estimation of L_V in the anisotropic case by means of vertical sections as on p. 416, as suggested by Gokhale (1990, 1992, 1993). The quantity $P_L(t)$ is then the mean number of intersections with projected fibres per unit test line length. The test lines are cycloids with minor axis *perpendicular* to the vertical axis.

Stoyan and Gerlach (1987) show how to determine the spatial curvature distribution function (the distribution function of curvature in the typical fibre point) from the planar curvature distribution function.

10.2.4 Stereology for excursion sets

Stereology for excursion sets as defined in Section 6.6.3 is extremely simple. The planar section of a spatial random field yields a planar random field. If the former is Gaussian then so is the latter. And both fields have the same mean and correlation function $k(r)$. Finally, for given level u the excursion sets of the spatial field and that of the planar field coincide on the section plane. Consequently, it suffices to estimate u and $k(r)$ for the planar excursion

set by means of the method sketched in Section 6.6.3 and all necessary spatial information is obtained.

10.2.5 On the precision of stereological estimators

The precision of stereological estimators, usually expressed by estimation variances, depends on the size of samples taken and on the spatial variability of the structure under investigation. The latter can be described by second-order characteristics. These are usually not known and must be estimated, often from the same samples as those for estimating the mean-value parameters.

The estimation of volume fraction is discussed in Section 6.4.2. The second-order characteristic needed there is the covariance $C(r)$. Hall and Ziegel (2011) developed bootstrap methods for a consistent estimation of the distribution of $\hat{V}_V$ and hence constructed, in various ways, confidence intervals for V_V.

In the case of stereological estimators based on counts of randomly distributed intersection points, it can be useful to employ the Poisson approximation. Then one can use the asymptotic confidence interval for the parameter of a Poisson distribution, as in Section 2.6.2, and so obtain confidence intervals for S_V, L_V and M_V. Thus, for example, an approximate $(1-\alpha)100\%$ confidence interval for S_V is given by

$$\frac{2}{l}\left(\sqrt{n}-\frac{z_{\alpha/2}}{2}\right)^2 \le S_V \le \frac{2}{l}\left(\sqrt{n+1}+\frac{z_{\alpha/2}}{2}\right)^2 \tag{10.19}$$

where l is the total length of the test lines employed, n the number of points of intersection of the surface with the test system, and $z_{\alpha/2}$ the $(1-\alpha/2)100^{\text{th}}$ percentile of the standard normal distribution.

More on statistics in stereology can be found in Ohser and Mücklich (2000), Beneš and Rataj (2004, Chapter 4) and Baddeley and Jensen (2005), as well as in the references therein.

10.3 Stereological mean-value formulae for germ–grain models

10.3.1 Planar sections

Suppose that Ξ_V is a spatial stationary germ–grain model and let $\{[x_n; \Xi_n]\}$ be the corresponding stationary germ–grain process, following the notation of Section 6.5. The distribution of the typical grain $\Xi_{V,0}$ is assumed to be rotation-invariant, but Ξ_V itself need not be isotropic. Consider the intersection Ξ_A of Ξ_V with an arbitrary test plane T,

$$\Xi_A = \Xi_V \cap T.$$

The position and normal direction of T can be chosen for convenience (because of the assumptions on Ξ_V), and so T is considered to be the (x_1, x_2)-plane. The intersection Ξ_A, if non-empty, is itself a planar germ–grain model.

The aim is to relate mean-value characteristics, such as the mean grain volume $\overline{V}$ and the germ-process intensity λ_V, of Ξ_V to the mean-value characteristics, such as the mean grain area $\overline{A}$ and germ-process intensity λ_A, of Ξ_A. (In the case of non-overlapping grains N_V is

the same as λ_V: the mean number of grains per unit volume. Analogous relationships hold for λ_A.)

The next two sections consider the problem of estimating shape and size distributions for the grains of Ξ_V from planar information, a so-called *unfolding problem*.

Throughout this section the grains of Ξ_V are assumed to be convex. This assumption is often made; it seems to be realistic in many cases and measurement difficulties arise when it does not hold, for example, when a nonconvex grain is intersected by the plane and the resultant planar grain is not connected. However, the basic Formula (6.122) has a generalised version holding for nonconvex particles, and so consideration of the nonconvex case is possible; see the discussion in Miles (1983, 1984). For the application of his results it is necessary to be able to decide whether different components of a section profile actually arise from the same grain.

Under the assumption of convex grains it is clear that the intersection Ξ_A is also a stationary germ–grain model with convex grains. Because the typical grain $\Xi_{V,0}$ of Ξ_V has rotation-invariant distribution, so has the typical grain $\Xi_{A,0}$ of the planar section structure. If Ξ_V is a Boolean model then so is Ξ_A; see Section 3.2.5.

Theorem 10.1. *If the grains are convex and the components of overlapping grains can be identified, the mean-value characteristics of Ξ_V and Ξ_A are connected by*

$$\lambda_V \overline{V} = \lambda_A \overline{A}, \tag{10.20}$$

$$\lambda_V \overline{S} = \frac{4\lambda_A \overline{L}}{\pi}, \tag{10.21}$$

$$\lambda_V \overline{\overline{b}} = \frac{\lambda_V \overline{M}}{2\pi} = \lambda_A, \tag{10.22}$$

where $\overline{\overline{b}}$ is the mean average breadth of the typical grain $\Xi_{V,0}$.

Proof. (Stoyan, 1979c) Consider the disc in the (x_1, x_2)-plane

$$c_r = \{\boldsymbol{x} = (x_1, x_2, x_3) : x_1^2 + x_2^2 \leq r^2, x_3 = 0\}.$$

By construction the numbers of grains hitting c_r must be the same for Ξ_V and Ξ_A, for all r. The corresponding mean values are given by Formula (6.124) as

$$\lambda_V \mathbf{E}\left(\nu_3(\check{\Xi}_{V,0} \oplus c_r)\right) = \lambda_V \left(\overline{V} + \frac{\pi \overline{S} r}{4} + \pi \overline{\overline{b}} r^2\right)$$

and

$$\lambda_A \mathbf{E}\left(\nu_2(\check{\Xi}_{A,0} \oplus c_r)\right) = \lambda_A(\overline{A} + \overline{L} r + \pi r^2)$$

for all $r \geq 0$. The ν_2-term in the second formula was calculated by means of the Steiner formula (1.23) and the ν_3-term in the first by means of the generalisation (6.29). Comparison of the coefficients of powers of r leads to the Formulae (10.20)–(10.22). □

There are more general formulae for d-dimensional germ–grain models intersected by k-dimensional flats: Formulae (3.66) and (3.67), given in Section 3.2.5 for the Boolean model, hold generally for stationary germ–grain models. Indeed, the formulae do not depend on assumptions such as independence of the grains or particular distributions for the germ process such as being a Poisson process.

The spatial characteristics λ_V, $\overline{V}$, $\overline{S}$ and $\overline{\overline{b}}$ cannot be determined directly from the formulae in the theorem. There are only three equations available for four unknowns. How to overcome this difficulty is a fundamental problem of classical stereology. Stereologists have tried to solve it by several tricks. One of them is to make use of *form factors* such as Blaschke's coefficients

$$f = \frac{4\pi\overline{S}}{\overline{M}^2}, \tag{10.23}$$

$$g = \frac{48\pi^2\overline{V}}{\overline{M}^3}. \tag{10.24}$$

The idea is to assume that f (or g) is known and fixed and so to reduce the number of unknowns to three.

The situation is not much easier even in the case of a Boolean model.

Example 10.1. *Planar section of a Boolean model*
The mean characteristics of a spatial stationary Boolean model Ξ_V with convex isotropic grains are

$$\lambda_V, \quad \overline{V}, \quad \overline{S} \quad \text{and} \quad \overline{M} = 2\pi\overline{\overline{b}}.$$

The planar section Ξ_A is again a Boolean model with mean characteristics

$$\lambda_A, \quad \overline{A} \quad \text{and} \quad \overline{L}.$$

These three mean values are connected with area fraction A_A, specific boundary length L_A and specific convexity number N_A^+ of Ξ_A by the formulae in Section 3.2.2:

$$A_A = 1 - \exp(-\lambda_A\overline{A}) = 1 - \exp(-\lambda_V\overline{V}), \tag{10.25}$$

$$L_A = \lambda_A\overline{L}\exp(-\lambda_A\overline{A}) = \lambda_V\frac{\pi}{4}\overline{S}\exp(-\lambda_V\overline{V}), \tag{10.26}$$

$$N_A^+ = \lambda_A\exp(-\lambda_A\overline{A}) = \lambda_V\overline{\overline{b}}\exp(-\lambda_V\overline{V}). \tag{10.27}$$

Again there are given three equations for the four unknowns λ_V, $\overline{V}$, $\overline{S}$ and $\overline{\overline{b}}$. The situation does not change if the specific connectivity number N_A is used.

If the grain distribution is given by a two-parameter distribution (e.g. spherical grains with lognormal distribution) then the equations above can be used to estimate these two parameters and λ_V; see the discussion in Section 3.4.3.

Another way to avoid this situation may be to use the disector. For example, the specific convexity number N_V^+ can be estimated by using this technique, as described in Bindrich and Stoyan (1991). Formula (3.49) gives N_V^+ as

$$N_V^+ = \lambda_V \exp(-\lambda_V \overline{V}). \tag{10.28}$$

10.3.2 Thick sections of spatial germ–grain models

The mean-value characteristics of Ξ_V can be related to those of the orthogonal projection Ξ^t of a thick section when Ξ_V is a motion-invariant germ–grain model. The formulae are

$$\lambda_V \left(\overline{V} + \frac{\overline{S}t}{4} \right) = \lambda_A \overline{A}, \tag{10.29}$$

$$\lambda_V \left(\frac{\pi \overline{S}}{4} + \pi \overline{\overline{b}} t \right) = \lambda_A \overline{L}, \tag{10.30}$$

$$\lambda_V (\overline{\overline{b}} + t) = \lambda_A. \tag{10.31}$$

The practical value of these formulae is limited since projections of non-intersecting grains may overlap and the determination of the parameters λ_A, $\overline{A}$ and $\overline{L}$ may be difficult.

Voss and Stoyan (1985) give a proof of these formulae which follows that of Theorem 10.1. The disc c_r there is replaced by the cylinder of height t

$$C_r = \{\boldsymbol{x} = (x_1, x_2, x_3) : x_1^2 + x_2^2 \le r^2, \quad 0 \le x_3 \le t\}.$$

Formula (10.29) is due to Cahn and Nutting (1959) and Formula (10.30) to DeHoff (1968).

The mean-value characteristics of the typical projected grain of Ξ_t are

$$\overline{A} = \frac{\overline{V} + \overline{S}t/4}{\overline{\overline{b}} + t} = \frac{4\pi \overline{V} + \pi \overline{S} t}{2\overline{M} + 4\pi t}, \tag{10.32}$$

$$\overline{L} = \frac{\pi \overline{S}/4 + \pi \overline{\overline{b}} t}{\overline{\overline{b}} + t} = \frac{\pi^2 \overline{S} + 2\pi \overline{M} t}{2\overline{M} + 4\pi t}, \tag{10.33}$$

see Voss (1980).

The formulae for the Boolean model in Section 3.2.2 give formulae for characteristics of Ξ^t if Ξ_V is a Boolean model. The formulae concern the area fraction $A_A(t)$, specific boundary length $L_A(t)$ and specific connectivity number $N_A(t)$:

$$A_A(t) = 1 - \exp\left(-\lambda_V\left(\overline{V} + \frac{\overline{S}t}{4}\right)\right), \tag{10.34}$$

$$L_A(t) = \pi\lambda_V\left(\frac{\overline{S}}{4} + \overline{\overline{b}}t\right)\exp\left(-\lambda_V\left(\overline{V} + \frac{\overline{S}t}{4}\right)\right), \tag{10.35}$$

$$N_A(t) = \left(\lambda_V\left(\overline{\overline{b}} + t\right) - \frac{\pi}{4}\lambda_V^2\left(\overline{\overline{b}}t + \frac{\overline{S}}{4}\right)^2\right)\exp\left(-\lambda_V\left(\overline{V} + \frac{\overline{S}t}{4}\right)\right), \tag{10.36}$$

as in Miles (1976).

The Equation system (10.29)–(10.31), as well as (10.34)–(10.36) and (10.25)–(10.27), has properties similar to those of the system (10.20)–(10.22). Again there are three equations and four unknown variables. One way of resolving this problem is to use two probes of different thicknesses t_1 and t_2 as proposed by Giger (1967) and Miles (1976); see also Weibel (1980). This approach has a disadvantage in that the resulting equations are ill-conditioned and sensitive with respect to measurement errors. Another possibility is to use a whole sequence of different probes with thicknesses $t_1, t_2, \ldots, t_n$ to measure the corresponding planar quantities and to determine the parameters of the spatial model by regression.

10.3.3 Tubular structures and membranes

It should be noted that there are also stereological methods which are related to spatial fibre and surface processes just as germ–grain models are related to point processes. These fibre- and surface-based models are systems of tubes and thin surfaces, for example tissue membranes. Stereological techniques yield V_V, S_V, L_V and so forth; see Gundersen (1979), Weibel (1980) and Baddeley and Averback (1983). Methods for the determination of the distribution of the thickness of membranes are presented in Ohser and Mücklich (2000).

10.4 Stereological methods for spatial systems of balls

10.4.1 Introduction

This section presents methods for a particular case of a stationary germ–grain model, namely, a random system of balls in $\mathbb{R}^3$. The case of planar sections is studied in detail while thick and linear sections are touched on briefly. The mathematical theory can apply to both the case of systems of non-overlapping balls and the case of systems of penetrable balls, under the condition that all balls, even in the case of overlapping, can be identified.

10.4.2 Planar sections and the Wicksell corpuscle problem

Theoretical solution

The following quantities can be determined from a planar section by means of the methods discussed in Section 6.5.7:

- N_A = the mean number of section discs per unit area,
- $D_A(r)$ = the distribution function of diameters of section discs.

The distribution function $D_A(r)$ always has a density function, denoted here by $\delta_A(r)$; the corresponding mean is denoted by d_A. The aim of stereology is to determine the following three-dimensional quantities:

- N_V = the mean number of balls per unit volume,
- $D_V(r)$ = the distribution function of the diameters of balls,
- d_V = the mean ball diameter.

Procedures for solving the important problem of determining $D_V(r)$ from knowledge of $D_A(r)$ are called *unfolding* procedures. The unfolding problem was first posed and theoretically solved by Wicksell (1925, 1926). However, as will become clear, there are serious statistical and numerical difficulties in implementing the solution.

The following formulae relate these quantities to each other:

$$d_V = \frac{\pi}{2}\left(\int_0^\infty \frac{\delta_A(r)}{r}\,\mathrm{d}r\right)^{-1}, \tag{10.37}$$

$$N_V = \frac{N_A}{d_V}, \tag{10.38}$$

$$D_V(r) = 1 - \frac{2d_V}{\pi}\int_r^\infty \frac{\delta_A(x)}{\sqrt{x^2 - r^2}}\,\mathrm{d}x \qquad \text{for } r \geq 0, \tag{10.39}$$

$$D_A(r) = 1 - \frac{1}{d_V}\int_0^\infty \left(1 - D_V\left(\sqrt{r^2 + x^2}\right)\right)\mathrm{d}x \qquad \text{for } r \geq 0, \tag{10.40}$$

$$N_A\big(1 - D_A(r)\big) = N_V \int_r^\infty \sqrt{x^2 - r^2}\,\mathrm{d}D_V(x) \qquad \text{for } r \geq 0. \tag{10.41}$$

Formula (10.38) is a particular case of (10.22) since $\bar{\bar{b}} = d_V$, and Formula (10.39) implies (10.37) with $r = 0$. If $D_V(r)$ possesses a density function $\delta_V(r)$ then

$$\delta_A(r) = \frac{r}{d_V}\int_r^\infty \frac{\delta_V(x)}{\sqrt{x^2 - r^2}}\,\mathrm{d}x \qquad \text{for } r \geq 0. \tag{10.42}$$

The solution of this Abel integral equation is

$$\delta_V(r) = -\frac{2d_V r}{\pi}\int_r^\infty \frac{1}{\sqrt{x^2 - r^2}}\frac{\mathrm{d}}{\mathrm{d}x}\left(\frac{\delta_A(x)}{x}\right)\mathrm{d}x \qquad \text{for } r \geq 0. \tag{10.43}$$

There are nice relations between the *moments* of $D_A(r)$ and $D_V(r)$ given by (10.67), presented in the context of thick sections below. When $t = 0$ these formulae specialise to the case considered here.

Drees and Reiss (1992) study the tail behaviour of $D_A(r)$ and $D_V(r)$. For example, they show that $D_A(r)$ and $D_V(r)$ belong to the same type of extreme value distributions (Fréchet, Weibull and Gumbel).

Example 10.2. *Particular forms of* $D_A(r)$
(a) Let the diameters of the balls be constant. Then Formula (10.40) implies

$$D_A(r) = 1 - \frac{\sqrt{d_V^2 - r^2}}{d_V}, \tag{10.44}$$

$$\delta_A(r) = \frac{r}{d_V\sqrt{d_V^2 - r^2}} \qquad \text{for } 0 \le r \le d_V.$$

The mean and variance of the section disc diameters are

$$d_A = \frac{\pi d_V}{4} \qquad \text{and} \qquad \sigma_A^2 = (32 - 3\pi^2)\frac{d_V^2}{48}. \tag{10.45}$$

These equations can be used to test whether the diameters are constant and if so, then to estimate d_V.

(b) If the diameters of the balls have a Rayleigh distribution, that is, if

$$\delta_V(r) = \frac{r}{a^2}\exp\left(\frac{-r^2}{2a^2}\right) \qquad \text{for } r \ge 0, \quad \text{with mean } d_V = a\sqrt{\frac{\pi}{2}}, \tag{10.46}$$

then the distribution reproduces itself:

$$\delta_V(r) = \delta_A(r) \qquad \text{for } r \ge 0. \tag{10.47}$$

This is the only distribution with this property; see Drees and Reiss (1992). It makes the use of the Rayleigh distribution attractive for stereology. The paper by Rysz and Wiencek (1980) gives an application of this idea.

(c) If the diameters have a uniform distribution on $[0, a]$, then

$$\delta_A(r) = \frac{2r}{a^2}\cosh^{-1}\left(\frac{a}{r}\right) \qquad \text{for } 0 \le r \le a, \tag{10.48}$$

see Ohser and Mücklich (2000, p. 170).

Before turning to the statistical problems in the determination of N_V, d_V and $D_V(r)$ by the above formulae a proof of Formulae (10.37)–(10.40) is presented, following Mecke and Stoyan (1980b).

Proof of Formulae (10.37)–(10.40). The system of balls can be described by a motion-invariant marked point process

$$\Psi_V = \{[x_n, y_n, z_n; d_n]\}.$$

Here (x_n, y_n, z_n) is the centre of the n^{th} ball and the mark d_n stands for its diameter. The corresponding intensity measure Λ_V (including the marks) has the form

$$\Lambda_V(B \times M) = N_V \nu_3(B) \mathscr{D}_V(M) \qquad \text{for Borel } B \times M \subset \mathbb{R}^3 \times [0, \infty),$$

where $\mathscr{D}_V$ denotes the mark distribution and ν_3 the volume measure. Thus $\mathscr{D}_V$ is the distribution of the diameter of the typical ball

$$\mathscr{D}_V([0, r]) = D_V(r) \qquad \text{for } r \geq 0.$$

All that is observed of a ball $[x, y, z; d]$ is its intersection with the (x, y)-plane. The condition that a section is not empty is precisely

$$4z^2 \leq d^2$$

and the resulting section diameter s is given by

$$s = \sqrt{[d^2 - 4z^2]^+},$$

where $[x]^+ = \max\{0, x\}$. Consider the system of all section discs. This can be described by another marked point process, which this time lies in the (x, y)-plane:

$$\Psi_A = \{[x_m, y_m; s_m]\}.$$

Its intensity measure Λ_A is given by

$$\Lambda_A(B' \times M') = N_A \nu_2(B') \mathscr{D}_A(M'), \qquad \text{for Borel } B' \times M' \subset \mathbb{R}^2 \times [0, \infty),$$

where $\mathscr{D}_A$ is the diameter distribution of the typical section disc (ignoring those of null section) and ν_2 the area measure, so

$$D_A(r) = \mathscr{D}_A([0, r]) \qquad \text{for } r \geq 0.$$

The value of $\Lambda_A(C)$ for the set $C = [0, 1) \times [0, 1) \times (r, \infty)$ can be expressed in two ways. First, the formula for Λ_A yields directly

$$\Lambda_A(C) = N_A\big(1 - D_A(r)\big).$$

Second, since the points of Ψ_A result from points of Ψ_V whose balls hit the (x, y)-plane, such points correspond to points $[x, y, z; d]$ of Ψ_V with

$$\left(x, y, \sqrt{[d^2 - 4z^2]^+}\right) \in C.$$

Therefore the expected number of Ψ_A points in C must equal the expected number of Ψ_V points for which the above is true:

$$\Lambda_A(C) = \mathbf{E}\left(\sum_{[x,y,z;d] \in \Psi_V} \mathbf{1}_C(x, y, w)\right),$$

where $w = \sqrt{[d^2 - 4z^2]^+}$. The formula for Λ_V and the Campbell theorem for marked point processes (4.20) yield

$$\begin{aligned}\Lambda_A(C) &= \int_{\mathbb{R}^3 \times [0,\infty)} \mathbf{1}_C(x, y, w)\, \Lambda_V\big(\mathrm{d}(x, y, z; d)\big) \\ &= N_V \int_0^\infty \mathscr{D}_V\left(\left(\sqrt{r^2 + t^2}, \infty\right)\right) \mathrm{d}t.\end{aligned}$$

Formula (10.38) is obtained by equating both expressions for $\Lambda_A(C)$, via

$$\mathscr{D}_V\big((u, \infty)\big) = 1 - D_V(u),$$

setting r equal to zero, and using

$$d_V = \int_0^\infty \big(1 - D_V(r)\big)\, \mathrm{d}r.$$

This yields Formula (10.40) immediately. Integration shows that (10.40) has as solution the result summarised in (10.39). Setting $r = 0$ in (10.39) gives (10.37). □

Determination of section disc diameters

The statistics begins with determination of the section disc diameters. Usually, these diameters are measured from profiles that are not exactly circular. Thus methods of image analysis are employed; see for example Balslev *et al.* (2000). A first step may be application of operations of mathematical morphology, to close gaps (closing) in the profiles and to separate aggregates of objects (opening). By the way, these 'objects' do not necessarily stand for single discs, since overlappings of balls in space and thus of section discs are possible. Thus aggregates of discs must be divided into single objects. For the resulting objects then 'centres' are determined (usually as centres of gravity) and finally discs with these centres are constructed such that the disc areas are equal to the areas of the former objects. This method is demonstrated in Kadashevich *et al.* (2005) for the case where the balls approximate partially overlapping pores. The edge-correction used here is minus-sampling.

The end result is a sample of n diameters $d_1, \ldots, d_n$ from a window W.

Simple mean-value estimators

A simple *ad hoc* estimator for d_V is based on Formula (10.37) and serves to deliver an initial example:

$$\hat{d}_V = \frac{n\pi}{2} \Big/ \sum_{i=1}^{n} \frac{1}{d_i}. \tag{10.49}$$

This estimator has been suggested by Saltykov (1950) and Fullman (1953). It has been studied by Watson (1971) and Franklin (1977, 1981). The latter constructed a confidence interval for d_V. It has been criticised on the grounds that its variance is infinite; see for example Ripley (1981, p. 210). Estimators for other moments of $D_V(r)$ have been studied in Nicholson (1970, 1976, 1978), Watson (1971) and Jakeman and Schaeffer (1978).

A counterpart to $\hat{d}_V$ is

$$\hat{N}_V = \frac{2}{n\nu_2(W)} \sum_{i=1}^{n} \frac{1}{d_i}. \tag{10.50}$$

Approaches to solve the unfolding problem

The determination of the distribution function $D_V(r)$ is an ill-posed problem of a well-known nature, which is typical for the inversion of integral equations of the first kind. Many statistical procedures have been developed to handle the ill-posed nature of the problem, which are all biased but lead to acceptable approximations. The work until 1995 is documented in SKM95; it seems that since then interest in the problem has faded out. A simple solution recommended in SKM95 seems to be the best solution; see below. For historical interest and to prevent rediscoveries the list of SKM95 is given here in abridged form:

(a) Discretisation of Formula (10.40) or (10.41) by discretising $D_V(r)$, which corresponds to grouping the sample. The integral is then approximated by a finite sum, and a finite system of linear equations is produced. Methods of this kind have been proposed by Goldsmith, Saltykov, Scheil, Schwartz, and Wicksell; see Lewis *et al.* (1973), Saltykov (1974) and Weibel (1980). Differences between the methods lie in choosing the representatives of the histogram classes: midpoints, upper or lower limits. A particular case is the following.

The Scheil–Schwartz–Saltykov method
As above, $\{d_1, \ldots, d_n\}$ is a sample of diameters of section discs in a planar section. An interval $(0, d_u)$ is chosen, with suitable upper limit d_u exceeding all the d_j. This interval is divided into k cells of width $\Delta = d_u/k$. The empirical number $\hat{n}_i$ of discs per unit area with diameters in $C_i = \big((i-1)\Delta, i\Delta\big]$ is recorded, for each $i = 1, \ldots, k$. The aim is to provide from $\{\hat{n}_1, \ldots, \hat{n}_k\}$ good estimates $\hat{N}_j$ for the expected number of balls per unit volume having diameters in C_j for $j = 1, \ldots, k$. The density of the distribution $D_V(r)$ can then be estimated as the histogram value $\hat{N}_j / \sum_{i=1}^{k} \hat{N}_i$ in the cell C_j.

If N_j is the expected number of balls per unit volume with diameters in C_j then in a plane section these balls contribute to the expected numbers n_i of section disc per unit area with diameters in C_i approximately as follows:

$$n_i = \Delta \sum_{j=i}^{k} b_{ij} N_j \qquad \text{for } i = 1, \ldots, k, \tag{10.51}$$

where the coefficients are

$$b_{ij} = \sqrt{j^2 - (i-1)^2} - \sqrt{j^2 - i^2}, \qquad \text{for } i \le j \text{ and } j = 1, \ldots, k, \tag{10.52}$$

Here the approximation is made that all balls contributing to n_i actually have diameter $j\Delta$. Note that other approximations, such as that the diameters are $j\Delta + \Delta/2$, or that they are uniformly distributed in $\big((j-1)\Delta, j\Delta\big)$, do not give better results.

Estimates $\hat{N}_j$ of the N_j can now be obtained by solving for N_j in these equations, using $\hat{n}_i$. The solutions have the form

$$\hat{N}_j = \frac{1}{\Delta} \sum_{i=1}^{k} c_{ji} \hat{n}_i, \tag{10.53}$$

where the c_{ij} may be obtained by back-substitution in the linear equations for n_i above.

As a by-product estimators for N_V and d_V are obtained:

$$\hat{N}_V = \sum_{j=1}^{k} \hat{N}_j \qquad \text{and} \qquad \hat{d}_V = \frac{n}{\hat{N}_V \nu_2(W)}. \tag{10.54}$$

(b) Application of Formula (10.39), replacing $D_A(r)$ by an empirical distribution function; see Blödner *et al.* (1984).

(c) Application of Formula (10.43) and use of spectral differentiation; see Anderssen and Jakeman (1975a,b).

(d) Parametric methods. These involve making a parametric assumption about the form of $D_V(r)$ and then estimating the parameters; see Likeš (1963), DeHoff (1965), Giger and Riedwyl (1970), Keiding *et al.* (1972) and Suwa *et al.* (1976).

The idea is simple: A parametric form of $\delta_V(r)$ is taken, whose parameters θ have to be estimated. The formula is plugged in (10.42), which leads to an expression for $\delta_A(r)$, where the same parameters θ as in $\delta_V(r)$ appear.

Assuming that the section disc diameters in the sample $\{d_1, \ldots, d_n\}$ can be considered as coming from independent random variables, one can maximise the likelihood function

$$L(d_1, \ldots, d_n; \theta) = \prod_{i=1}^{n} \delta_A(d_i; \theta) \tag{10.55}$$

with respect to θ, usually by means of numerical methods, to yield estimates of θ.

(e) Trial and error methods, which consist of guessing a diameter distribution $D_V^{(1)}(r)$, computing the corresponding $D_A^{(1)}(r)$, comparing this with the empirical $D_A(r)$, and then making a second guess at the diameter distribution, and so forth; see Voss and Schubert (1975).

(f) Regularisation. This popular and powerful method has been also applied to the particular case of the Wicksell problem. In the case of estimation of the probability density function, let $\hat{\delta}_A(r)$ be an empirical density function of the section disc diameters, and let $\delta_A^*(r)$ be the function obtained by means of Formula (10.42) with a $\delta_V(r)$ which depends on some parameters. In a naïve solution method the parameters are determined by minimising

$$S = \int_0^\infty \left(\hat{\delta}_A(r) - \delta_A^*(r)\right)^2 \mathrm{d}r.$$

The idea of regularisation is to introduce the term

$$d = \int_0^\infty \left(\delta_V''(r)\right)^2 \mathrm{d}r$$

and to minimise

$$S + \varepsilon d$$

for a suitable positive ε. The additional term helps to find smooth solutions, which can be easily interpreted. Typical references for the application of regularisation in the Wicksell problem are Nychka (1983b,a), Nychka *et al.* (1984) and Weese (1995).

(g) EM algorithm. Wilson (1987) and Silverman *et al.* (1990) used modified forms of the EM algorithm; see also Reiss (1993, pp. 163–7) and Ohser and Mücklich (2000, pp. 185–6). The standard EM algorithm consists of two steps, an **E**xpectation-step and a **M**aximisation-step; see McLachlan and Krishnan (2008). The latter belongs to maximum-likelihood estimation. The modification consists in adding a smoothing-step. To justify the maximisation-step these authors assume that the ball centres form a homogeneous Poisson point process. Instead it is better to interpret the M-step as a Moment-method-step. There seems to be no convergence proof as yet, but practical experience shows that the method works even when the Poisson process assumption is inappropriate.

(h) Kernel methods. Taylor (1983) used a kernel estimator with variable bandwidth for the density $\delta_A(r)$ and then determines $\delta_V(r)$ by means of Formula (10.43); see also Möller (1989). Hall and Smith (1988) used a kernel estimator for the density function of the squared disc diameters in order to obtain the density function of the squared ball diameters. For the squared diameters the integral equation is easier. Van Es and Hoogendoorn (1990) postponed the kernel smoothing until after a transformation step. They determined first an estimator $D_V(r)$ by means of Formula (10.39) and then derived an estimator of $\delta_V(r)$ by kernel smoothing. Weese (1995) discussed the relationship of kernel methods and regularisation techniques, and Weese *et al.* (1997) combined the advantages of both.

(i) Wavelet method. Antoniadis *et al.* (2001) demonstrated the application of wavelet methods. The authors first converted the integral equation to a form suitable for the application of thresholding wavelet methods. Then they derived the asymptotic properties of their estimators and compared with other numerical methods.

(j) Nonparametric maximum likelihood; see van Es (1991) and Jongbloed (1991).

(k) Particular integration methods. Mase (1995) suggested rewriting the integral in Formula (10.39) as

$$\int_{-1}^{1} \frac{|x|}{\sqrt{1-x^2}} \delta_A(x)\,\mathrm{d}x$$

and then using the Gauss–Chebyshev quadrature method and a smoothing technique for the empirical $D_A(r)$.

No method has clear advantages over all others. Statistical and numerical difficulties interact in a delicate fashion.

The two-step method

The authors recommend a *two-step method* as also in other places of this book.

- First step: Apply one of the numerical methods above as a pilot study, in order to generate a plausible assumption on the type of the density function $\delta_V(r)$. Since only a qualitative problem is solved, high precision is not necessary. Indeed, even biased estimators may be useful here.
- Second step: Use a parametric method, preferably the maximum likelihood method, for the estimation of the parameters of $\delta_A(r)$ obtained via Equation (10.42). It is important to note that statistics should be based only on the diameters d_i of the section discs, as these produce the only (relatively) safe data.

In view of Ohser and Mücklich (2000, Tables 6.6–6.7), it is suggested to use for the first step the classical Scheil–Schwartz–Saltykov method; see (a) above, perhaps in the improved form of EM algorithm. Note that in that book there are source codes for the numerical calculation.

The application of this method is demonstrated in various papers; see for example Groos and Kopp-Schneider (2006) and Kadashevich *et al.* (2005). In the latter paper the spatial diameter distribution is a mixture of an exponential distribution (for very small pores) and normal distribution (for larger pores).

10.4.3 Linear sections

The following quantities are available from a linear section:

- N_L = mean number of chords per unit length,
- $D_L(r)$ = distribution function of chord lengths.

The distribution function $D_L(r)$ always has a density, denoted by $\delta_L(r)$.

The aims of statistical analysis in the case of linear unfolding are the same as in the case of planar unfolding. The mathematical problem of establishing relationships between N_L and $D_L(r)$ on the one hand and N_V and $D_V(r)$ on the other was solved by Spektor (1950) and Lord and Willis (1951). The following formulae can be proved in a way similar to that of the planar case:

$$N_V = \frac{4N_L}{\pi d_V^{(2)}}, \tag{10.56}$$

$$D_V(r) = 1 - \frac{d_V^{(2)}}{2}\frac{\delta_L(r)}{r}, \tag{10.57}$$

$$D_L(r) = \frac{2}{d_V^{(2)}}\int_0^r x\big(1 - D_V(x)\big)\,\mathrm{d}x, \tag{10.58}$$

$$N_L\big(1 - D_L(r)\big) = N_V\frac{\pi}{4}\int_r^\infty (x^2 - r^2)\mathrm{d}D_V(x) \qquad \text{for } r \geq 0, \tag{10.59}$$

where $d_V^{(2)}$ denotes the second moment of $D_V(r)$. Formula (10.56) can be interpreted as a particular case of Formula (10.3) since the mean ball surface is $4\pi d_V^{(2)}$.

Example 10.3. *Particular forms of $D_L(r)$*
(a) If the ball diameters are constant then by (10.58)

$$D_L(r) = \frac{r^2}{d_V^2}, \tag{10.60}$$

$$\delta_L(r) = \frac{2r}{d_V^2} \qquad \text{for } 0 \le r \le d_V. \tag{10.61}$$

The mean chord length satisfies

$$d_L = \frac{2d_V}{3}. \tag{10.62}$$

(b) As in the case of planar sections, the Rayleigh distribution has a reproduction property:

$$D_V(r) = D_L(r) \qquad \text{for } r \ge 0.$$

(c) Let the ball diameters have an exponential distribution with parameter μ. Then

$$D_L(r) = 1 - (1 + \mu r)\exp(-\mu r),$$

$$\delta_L(r) = \mu^2 r \exp(-\mu r) \qquad \text{for } r \ge 0.$$

Relation (10.57) implies that

$$d_V^{(2)} = 2 \lim_{r \downarrow 0} \left(\frac{r}{\delta_L(r)} \right).$$

Consequently a density function $f(r)$ is a chord length density function only if

$$0 < \lim_{r \downarrow 0} \left(\frac{f(r)}{r} \right) = f'(0) < \infty. \tag{10.63}$$

Among the family of gamma (or Schulz) distributions with densities

$$f(r) = \frac{\mu^\alpha r^{\alpha-1}}{\Gamma(\alpha)} \exp(-\mu r) \qquad \text{for } r \ge 0 \text{ and } \alpha \ge 0,$$

the condition given in (10.63) is fulfilled only when $\alpha = 2$, that is, when the ball diameters have an exponential distribution.

The linear section method is more unstable than the planar section method. Tests suggest that 'it should not be used whenever planar sectioning is possible'; see Ripley (1981, p. 212). Measurement errors and statistical errors play a still greater rôle. Ohser and Mücklich (2000, p. 175) present methods for numerical solution.

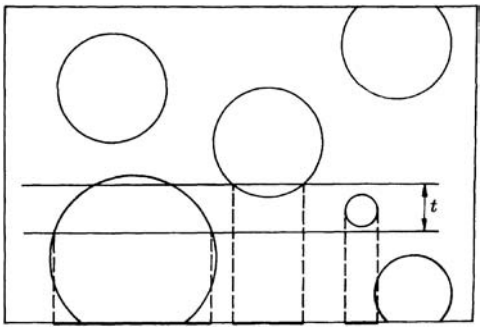

Figure 10.3 A thick section through a system of opaque balls lying in a transparent medium. The projections are shown at the bottom of the window.

10.4.4 Thick sections

In this section a system of opaque balls embedded in a transparent medium is considered. The system is intersected by two parallel planes separated by (a small) distance t. Only the projection of the part of the system lying between the two planes is observed, as in Section 10.2.3; see Figure 10.3. The contrary case, studied by Coleman (1981, 1982, 1983), is when the balls are transparent and the medium is opaque, as would be the case for holes in Swiss cheese or closed foams.

Just as in the case of planar sections one obtains relationships between $N_A(t)$ and $D_{A,t}(r)$ on the one hand and N_V and $D_V(r)$ on the other. However, the planar quantities must be interpreted more carefully: $D_{A,t}(r)$ is the distribution function of the *projection* disc diameters, where all projections are counted, also such which are completely overlapped ('overprojection') by larger projections; $N_A(t)$ is the corresponding number density.

Bach (1965, 1967, 1976), Crompton *et al.* (1966) and Mecke and Stoyan (1980b) studied this problem. Bach showed that the solution for $D_V(r)$, which is surely only of theoretical value, is

$$D_V(r) = 1 - \frac{t\big(1 - D_{A,t}(r)\big) - \int_r^\infty p\left(\frac{\sqrt{\pi}}{\sqrt{2}t}\sqrt{x^2 - r^2}\right) \frac{1 - D_{A,t}(x)}{\sqrt{x^2 - r^2}}\, x\, \mathrm{d}x}{t - \int_0^\infty p\left(\frac{\sqrt{\pi}x}{\sqrt{2}t}\right)\big(1 - D_{A,t}(x)\big)\, \mathrm{d}x} \qquad \text{for } r \geq 0, \tag{10.64}$$

where $p(x)$ is given by

$$p(x) = 1 - \exp(x^2/2) \int_x^\infty \exp(-t^2/2)\, \mathrm{d}t \qquad \text{for } x \geq 0. \tag{10.65}$$

The intensity N_V satisfies

$$N_V = \frac{N_A(t)}{(d_V + t)}. \tag{10.66}$$

Bach (1959, 1967) found some important relationships between the moments of $D_V(r)$ and $D_{A,t}(r)$. (In the case $t = 0$ they reduce, of course, to those for planar sections.) Let

$$M_1 = d_V,$$

$$M_k = \int_0^\infty x^k \, \mathrm{d}D_V(x) \quad \text{and} \quad m_k = \int_0^\infty x^k \, \mathrm{d}D_{A,t}(x) \qquad \text{for } k = 0, 1, 2, \ldots.$$

Then the moment relationships are

$$(t + d_V)\, m_k = J_{k+1} M_{k+1} + t M_k, \tag{10.67}$$

where

$$J_r = \frac{\sqrt{\pi}}{2} \cdot \frac{\Gamma(r/2 + 1/2)}{\Gamma(r/2 + 1)} \qquad \text{for } r = 1, 2, \ldots.$$

The numerics of the unfolding problem is discussed in Ohser and Mücklich (2000, pp. 193–8).

10.4.5 Sieving distributions for balls

Sieving distributions for balls are a particular case of the volume-weighted distributions discussed in Section 6.5.5. Such distributions can often be more interesting than the number-weighted distributions such as $D_V(r)$. This is the case when it is important to know the fraction of volume corresponding to a certain class of diameters; a few very big balls may be more important than many tiny balls.

Let $D_V^S(r)$ be the volume-weighted or *sieving diameter distribution*. The quantity $D_V^S(r)$ is the total volume of balls of diameter less than or equal to r (per unit volume) divided by the total volume of all balls (again per unit volume). This is related to $D_V(r)$ itself in a manner familiar from Section 6.5.5; the corresponding densities satisfy

$$\delta_V^S(r) = r^3 \delta_V(r) \Big/ \int_0^\infty x^3 \delta_V(x) \, \mathrm{d}x \qquad \text{for } r \geq 0. \tag{10.68}$$

More on sieving (and more general, on weighted) distributions can be found in Ohser and Mücklich (2000, Section 7.5). For example, there (p. 225) is an integral equation connecting the volume-weighted ball diameter distribution with the area-weighted section disc diameter distribution. The numerics is here more stable than for the nonweighted distributions.

10.5 Stereological problems for nonspherical grains (shape-and-size problems)

10.5.1 General remarks

Section 10.4 demonstrates that stereology gives rise to hard problems if more is required than mean values; and these difficulties arise already in the simple case of spherical grains. The case of nonspherical grains is even more complicated. Here the section figures or *profiles* have varying shapes and it is often difficult to make even inferences about the true three-dimensional

shape. The size distribution cannot be investigated at all without some information about the shape of the grains. But if such information is given, it helps to introduce an additional parameter (such as the number of vertices of a polygonal section profile), which may stabilise the unfolding procedure.

A popular procedure is to approximate the grains by spherical grains matched in some way so as to be 'equivalent'. For example, the areas of the section profiles can be measured and thus diameters calculated for section discs with the same areas. This method may sometimes produce fairly accurate results but can also yield nonsense. Wicksell (1926) first suggested this method.

In this section two important special cases are considered which are often considered in the literature: those of ellipsoidal and polyhedral grains. Under shape assumptions such as these it is formally possible to write down integral equations for the size distributions; see for example Cruz-Orive (1976, 1978), Ohser and Mücklich (2000) and Nagel (2010).

It is generally assumed that the structure considered is a motion-invariant germ–grain model. Note that this can be more general than a system of isolated and independent grains, for example, the cells of a tessellation also produce a germ–grain model. So long as only shape and size of grains is of interest, the following theorem shows how to proceed.

Theorem 10.2. *(Stoyan, 1982) Let Ξ be a motion-invariant germ–grain model with typical grain Ξ_0. Consider the intersection of Ξ with an arbitrary plane or line independent of Ξ. Let Ξ_0^S be the typical grain of the planar or linear germ–grain model resulting from the section. Then Ξ_0^S has a distribution that is independent of any assumptions concerning the distribution of the point process of germs and the correlations between germs and grains.*

Consequently, in order to obtain a stereological integral equation between spatial and sectional characteristics of the individual grains there is no loss of generality in assuming that the germs form a homogeneous Poisson process, that the grains are independent, and that sections of different grains are distinguishable when they overlap. Furthermore, for obtaining the distribution of Ξ_0^S it is sufficient to determine the distribution of the section profile of a single typical grain intersected by a Poisson line or plane process.

Planar sections

For the case where all grains are convex and have the same shape but different sizes, Ohser and Mücklich (2000, Equation (7.1)) gave a general integral equation, which is presented as Formula (10.69) below. They used a size characteristic, measured in length, for the grains, such as their average or maximum breadth. For brevity in this section the chosen size characteristic will simply be called size, and its distribution function is denoted by $F_V(a)$. The mean number of grains per volume unit is N_V.

The corresponding characteristics for a planar section are the profile-size distribution function $F_A(a)$ and the grain-profile intensity N_A.

The standard grain has size 1 and (deterministic) average breadth $\overline{b}_\mathrm{s}$. (If the standard grain is a ball and size characteristic is the maximum breadth, then $\overline{b}_\mathrm{s} = 1$.)

The integral equation, which connects $F_V(a)$ and $F_A(a)$, is

$$N_A\big(1 - F_A(a)\big) = N_V \overline{b}_\mathrm{s} \int_a^\infty u\big(1 - G_u(a)\big)\mathrm{d}F_V(u) \qquad \text{for } a \geq 0. \tag{10.69}$$

where $G_u(a)$ is the conditional size distribution of section profiles of a grain of size u. The kernel function $p(u, a) = \overline{b}_s u\big(1 - G_u(a)\big)$ in (10.69) depends on grain shape. In the case of spherical grains it is explicitly given by Formula (10.40).

Formula (10.69) implies Formula (10.22) with $a = 0$.

The analytical determination of the kernel is usually difficult. Thus simulation is used: the typical grain is intersected by random planes (so-called IUR-planes: isotropic uniform random planes) and the section profiles are evaluated; see Ohser and Mücklich (1995; 2000, p. 204).

For the numerical determination of $F_V(u)$ a similar procedure as in the case of spherical grains is recommended: the two-step method, where in the first step ideas of the EM algorithm should be used; see Ohser and Mücklich (2000, pp. 208 and 218).

Linear sections

Linear sections are sometimes of interest when there is no other way to get spatial information. In particular, scattering investigations lead to chord length distributions; see p. 23. In the following the same setting as for planar sections is assumed. All grains have the same shape, but their sizes are random, represented by some size characteristic measured in length with probability density function $f_V(a)$. The second moment of the size is $\overline{a^2}$. The chord length distribution function of a grain with size a is denoted by $L_a(l)$. It is assumed that it is known; see the references in Section 1.7.3. The following integral gives the distribution function $L(l)$ of the lengths of chords through the germ–grain model considered:

$$L(l) = \int_0^\infty L_a(l)\, a^2 f_V(a)\, \mathrm{d}a \Big/ \overline{a^2}. \tag{10.70}$$

The term $a^2 \big/ \overline{a^2}$ yields the necessary weighting: larger grains are intersected more frequently than smaller ones, and so area weighting should be used, since Cauchy's formula says that the mean area $\mathbf{E}(F)$ of a random orthogonal projection of a convex body K with surface area $S(K)$ satisfies

$$\mathbf{E}(F) = \frac{1}{4} S(K);$$

see Santaló (1976, p. 218). Typically, there is a maximum length $l(a)$ with the property $L_a(l) = 1$ for $l > l(a)$. This makes the explicit form of the integral in (10.70) a bit difficult. For the particular case of spherical grains Formula (10.70) yields (10.58). There the size characteristic is the diameter and $\overline{a^2}$ corresponds to $d_V^{(2)}$ and $f_V(a)$ to $\delta_V(r)$. The maximum length is $l(a) = a$ and

$$L_a(l) = \begin{cases} \dfrac{l^2}{a^2} & \text{for } 0 \le l \le a, \\[2ex] 1 & \text{otherwise.} \end{cases}$$

10.5.2 Two particular grain shapes

Ellipsoids

Ellipsoids form a frequently studied case of nonspherical grains. Here the stereologist wants to determine the joint distribution of size and shape. Cruz-Orive (1976, 1978) gives an excellent introduction to work done up to 1976 (dating back to Wicksell, 1926). As Cruz-Orive points out, it is not possible to solve completely the general problem of reconstructing from planar sections the shape and size distribution of ellipsoids. One must assume either restrictions on the form of the ellipsoids (for example, that the ellipsoids are all spheroids, that is, ellipsoids of revolution) or restrictions on the orientation of the ellipsoids relative to the plane of intersection. Cruz-Orive (1976) presents an example employing on the one hand oblate and on the other hand prolate spheroids, that is, ellipsoids of revolution generated by ellipses revolving around their major and minor axes respectively; in either case the same collection of planar elliptical section figures is produced. This settles a conjecture of Moran (1972) that the general ellipsoidal problem is undetermined.

In the case of spheroids Cruz-Orive (1976) derives and solves an integral equation connecting the bivariate densities of principal semi-axes and eccentricity parameters of ellipses. Flynn *et al.* (2009) use a parametric approach (normal distribution) and maximum likelihood estimation in the context of spatial analysis of mitochondrial networks.

Cruz-Orive (1978) suggests estimation of the size–shape bivariate histogram of spheroids from the corresponding histogram of elliptical parameters measured in the plane of intersection. Using numerical experiments Cruz-Orive concludes that the spherical approximation is acceptable when the ratio of minor axis to major axis is greater than 0.7. The book by Weibel (1980) is still an excellent reference to stereology of ellipsoids.

Beneš and Krejčíř (1997), Beneš *et al.* (1997) and Beneš and Rataj (2004, Chapter 6) consider stereological unfolding of the trivariate size–shape–orientation distribution for the case of spheroids.

Convex polyhedra

The case of polyhedral grains is rather complicated. This will be appreciated immediately if the reader considers that the shape of an intersection profile varies considerably depending on the plane of intersection. For example, for a parallelepiped the intersection profiles can be polygons with 3, 4, 5, or 6 sides; see Figure 8.4 on p. 300.

The literature is devoted to the shape and the size problem. There is a general theory for an important aspect of the shape problem: determination of the probabilities p_n that the typical intersection profile has n sides. This has been developed by Ambartzumian (1974b, 1982), Sukiasian (1982) and Voss (1982). Ambartzumian's method (also used by Sukiasian) is based on his solution of the Buffon–Sylvester problem in $\mathbb{R}^3$, and it studies random plane sections through systems of needles, where the needles correspond to the edges of the polyhedron. His 1973 paper gives the probabilities for the cube. Voss and Sukiasian tabulate p_n for various polyhedra. Table 10.2 displays some of their results. Sukiasian (1982) finds some equations and inequalities that the p_n must satisfy.

Solutions of the size problem assume that shape is known. Then chord length or section area distributions may help determine the size distribution. For chord lengths see the references in Section 1.7.3. The corresponding distributions are rather complicated; see for example

Table 10.2 The probability p_n that the number of sides of a random section of a polyhedron is n.

Polyhedron	Height to side length ratio	Number of sides of section profile					
		3	4	5	6	7	8
Regular tetrahedron		0.711	0.289	—	—	—	—
Regular triangular pyramid with	1	0.715	0.285	—	—	—	—
height to side length ratio of:	2	0.774	0.226	—	—	—	—
Cube		0.280	0.487	0.187	0.046	—	—
Parallelepiped with square base and	2	0.248	0.536	0.183	0.033	—	—
height to side length ratio of:	4	0.180	0.653	0.152	0.014	—	—
Regular hexagonal straight prism	1	0.145	0.525	0.235	0.088	0.005	0.001
with height to side length ratio of:	8	0.109	0.206	0.193	0.421	0.066	0.005

Figure 10.4. Ohser and Mücklich (2000, Sections 7.4 and 8.1.2) study in detail the cases of cubic and prismatic grains, starting from planar sections.

Other candidates for polyhedral grains are the typical cells of the Poisson plane ('Poisson polyhedron') and Poisson-Voronoi tessellations. Note that the typical planar profile of the Poisson polyhedron is the Poisson polygon. Consequently the formulae for this polygon, such as the p_n tabulated in Table 9.2 on p. 372, can be employed. The typical planar profile of the Poisson-Voronoi tessellation is much more complicated; see the next section.

10.6 Stereology for spatial tessellations

The intersection of a motion-invariant spatial tessellation by a plane is a planar tessellation. Its main parameters can be estimated and by the standard stereological formulae transformed in characteristics of the spatial tessellation:

$$N_V \bar{\bar{b}} = N_A(\text{cells}), \tag{10.71}$$

$$S_V = \frac{4}{\pi} L_A(\text{edges}), \tag{10.72}$$

$$L_V = 2P_A(\text{vertices}). \tag{10.73}$$

If the mean number of plates emanating from the typical edge is 3 for the spatial tessellation then the mean number of edges emanating in a typical vertex is also 3 for the planar tessellation.

The disector described in Section 6.5.7 can be applied for tessellations to estimate N_V, the mean number of cells per volume unit. This is described in Liu *et al.* (1994).

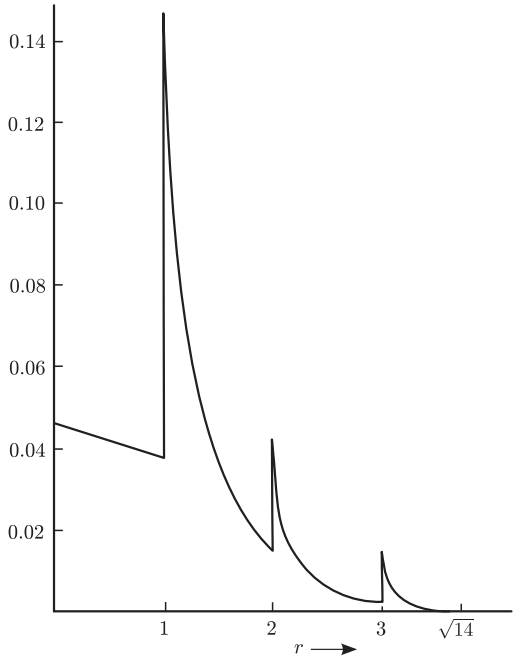

Figure 10.4 Probability density of length of random chords for a parallelepiped with side lengths 1, 2 and 3. The curve was computed by a program written by Gille (1988).

If the spatial tessellation is a *Poisson-Voronoi tessellation* with parameter λ_3 (the mean number N_V of cells per unit volume, in Chapter 9 denoted by ϱ) then for the resulting planar tessellation

$$n_{02} \equiv 3 \text{ almost surely}, \qquad \overline{n}_{20} = 6,$$

where n_{02} is the number of cells adjacent at the typical vertex and $\overline{n}_{20}$ the mean number of vertices (edges) of the typical cell. The planar densities above are

$$N_A(\text{cells}) = 1.46\lambda_3^{2/3}, \tag{10.74}$$

$$L_A(\text{edges}) = 2.29\lambda_3^{1/3}, \tag{10.75}$$

$$P_A(\text{vertices}) = 2.92\lambda_3^{2/3}. \tag{10.76}$$

Because of (9.26), which means $2N_A = P_A$ in the given case, (10.74) and (10.76) say the same. Further characteristics of the planar section tessellation are given by

$$\lambda_1^{(2)} = 4.37\lambda_3^{2/3}, \qquad \bar{l}_1 = 0.52\lambda_3^{-1/3}, \tag{10.77}$$

$$\bar{l}_0 = 1.57\lambda_3^{-1/3}, \qquad \overline{a_2^2} = 0.70\lambda_3^{-4/3}, \tag{10.78}$$

where $\lambda_1^{(2)}$ is the mean number of edges per area unit, $\bar{l}_1$ the mean length of the typical edge, $\bar{l}_0$ the mean length of edges emanating at the typical vertex, and $\overline{a_2^2}$ the second moment of area of the typical cell.

Formulae (10.74)–(10.76) offer methods for estimating $\lambda_3 = N_V$, for example

$$\hat{N}_V = 0.20 \hat{P}_A^{3/2}, \tag{10.79}$$

by counting planar vertices. Hahn and Lorz (1994a) and Lorz (1995) investigate biases and estimation variances of these estimators. They show that the biases are small and the variances are practically the same for all three estimators. The coefficient of variation ($= \sqrt{\text{variance}}/\text{mean}$) is approximately $1/\sqrt{n}$, where n is the number of cells observed in the planar sampling window. Consequently, the estimator based on counting vertices given by Formula (10.79) is preferable; its application does not require an edge-correction.

Example 10.4. *Austenite grain boundaries in steel*
This is a continuation of Example 9.2 on p. 394. Figure 9.17(a) shows the boundaries of Austenite grains in a section through some steel. The cells in the figure are not convex but it seems appropriate to approximate them by convex polygons as in Figure 9.17(b). For this, the following values were obtained using the methods discussed in Section 9.10.3

$$\hat{N}_A = 0.34, \qquad \hat{L}_A = 0.96, \qquad \hat{P}_A = 0.69,$$

with length unit as in Figure 9.17(b). Under the assumption that the planar tessellation is a planar section of a spatial Poisson-Voronoi tessellation the corresponding parameter λ_3 can be estimated using N_A, L_A and P_A. The formulae above give the values 0.112, 0.074 and 0.115 (note that $2N_A = P_A$, without '$\wedge$') as estimates for λ_3. The discrepancy between these values throws doubt on whether the pattern really corresponds to a section of a Poisson-Voronoi tessellation. Conceivably a parametric bootstrap test could be conducted to decide whether the fluctuations are significant or whether they are consistent with the spatial Poisson-Voronoi tessellation assumption.

Comparison between Figures 9.7 and 9.17(a) suggests that a variant of the Johnson–Mehl model might be appropriate; note in particular the curved boundaries, their concavity for large grains and the clusters of small grains. This might be the result of two stages of generation of Austenite-grain germs. Saltykov (1974, Chapter 2) gives an interesting and relevant discussion.

Note that the planar section of a Poisson-Voronoi tessellation is not a planar Poisson-Voronoi tessellation. This is obvious since the formulae above give $L_A^2/P_A = 1.80$ for the section tessellation while $L_A^2/P_A = 2$ for the planar Poisson-Voronoi tessellation. Figure 10.5 shows a planar section through a simulated Poisson-Voronoi tessellation. It cannot be a Dirichlet tessellation generated by some point pattern because of the occurrence of very small cells as neighbours of large cells in opposite positions. The existence of such configurations can be used to prove that planar sections of Poisson-Voronoi tessellations cannot be Dirichlet tessellations; see Chiu *et al.* (1996).

However, Voronoi tessellations belong to the class of Laguerre tessellations. A planar section of a Laguerre tessellation is a Laguerre tessellation, and thus the planar section of a Voronoi tessellation is a Laguerre tessellation (Nagel, 2010).

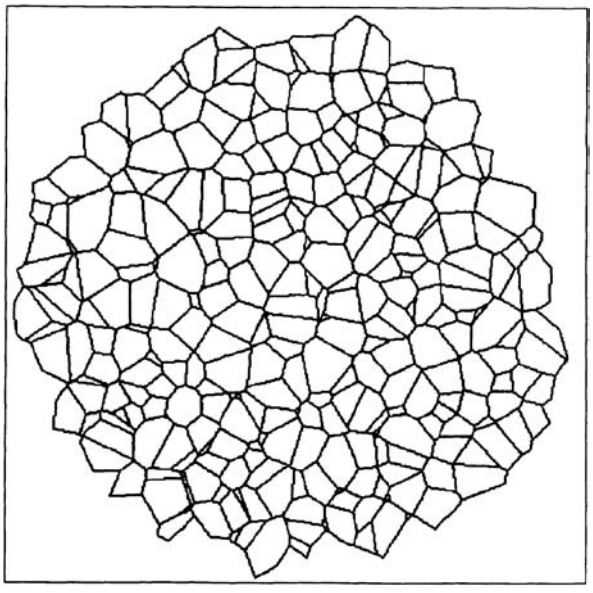

Figure 10.5 Planar section through a Poisson-Voronoi tessellation. Inspection shows that this tessellation cannot be produced by a Dirichlet tessellation of a point-pattern because of the occurrence of very small cells as neighbours of large cells in opposite positions.

If the real structure deviates from the Poisson-Voronoi model then of course the methods above become inaccurate. Perhaps the estimator using N_A is then still the best.

Tests of the hypothesis that a given tessellation is a Poisson-Voronoi tessellation are suggested and discussed in Hahn and Lorz (1994b), based only on planar sections. If the alternative hypotheses are Voronoi tessellations relative to other point processes then tests based on the variability of section cell area seem to be most powerful.

Perhaps surprisingly, mean-value characteristics of planar sections of Voronoi tessellations relative to non-Poisson processes may not differ very much from those corresponding to Poisson-Voronoi tessellations. This and practical experience suggest that good estimates of N_V for arbitrary spatial tessellations can be obtained by the following method: Obtain the empirical N_A from planar sections, plug it into Formula (10.74) to get the corresponding λ_3, and use the latter as an estimate of N_V, under the working assumption that the given tessellation is in some aspects not 'far from' a Poisson-Voronoi tessellation.

Schwertel and Stamm (1997) applied this method (and others) to samples of austenitic steel. They found that N_V can reliably estimated in this way, but it 'is not sufficient in predict the higher moments reliably'. Coster *et al.* (2005) made a similar study for cerine, a sintered ceramic, CeO_2, which led them to a particular Johnson–Mehl model.

An analogous approach is possible for linear sections: the mean number of intersections of cell faces with a test line per unit length is

$$P_L = 1.456\lambda_3^{1/3}. \tag{10.80}$$

It is easy to see that sections of stationary STIT tessellations inherit the STIT property. In particular, a linear section yields a one-dimensional Poisson point process. Furthermore, the

distribution of any stationary STIT tessellation is uniquely determined by its intensity (S_V, L_A or P_L, respectively) and the directional distribution of the cell boundaries. Thus the stereological problems are reduced to the estimation of these characteristics and are quite similar to those in the case of a Poisson plane tessellation. For motion-invariant STIT tessellations it suffices to use just one of the fundamental mean-value formulae.

Lorz (1990) studies the distribution of cell areas of the planar section tessellations of spatial Voronoi tessellations with respect to Poisson, Matérn cluster and hard-core processes. This is continued by Lorz and Hahn (1993) and van de Weygaert (1994), the latter also considers form factors, boundaries and edges.

If the spatial tessellation is a *Poisson plane tessellation* with parameter $\varrho = S_V/2$, then the planar section is a Poisson line tessellation with the same parameter ϱ, which in the planar context is the mean number of lines hitting a test line segment per unit length. The quantity $N_A(\text{cells})$ can be used to estimate ϱ by

$$\varrho = 2\sqrt{N_A(\text{cells})/\pi}. \tag{10.81}$$

Note that

$$N_V = \frac{\pi\varrho^3}{6}. \tag{10.82}$$

Ohser and Mücklich (2000, Section 8.2 and Chapter 10) describe stereological analysis of general tessellations based on the fact that the cells are polyhedra, using stereological methods for polyhedra as in Section 10.5.2.

A further problem for tessellations in $\mathbb{R}^3$ concerns the determination of the distribution of the angles between the plates or facets at the typical edge. Under 'equilibrium conditions' one would expect an angle of 120°; see Saltykov (1974) and Harker and Parker (1945). If the angles are constant at 120° then the distribution of the angle at the typical vertex in the planar section tessellation can be calculated under the assumption of stationarity and isotropy; the mean is again 120° and the standard deviation is 22°. Duvalian (1971) calculates the standard deviations for other spatial angles, both larger and smaller than 120°. The inverse problem of estimating the spatial angle distribution given the angle distribution in a planar section is an interesting problem of stereology; see Schwandtke (1985) and Miles (1987).

10.7 Second-order characteristics and directional distributions

10.7.1 Introduction

Previous sections describe stereological methods that yield mean values or distributional information on particles. However, more is possible: the spatial variability of three-dimensional structures can also be explored stereologically. In one case this was already explained: As Section 10.2.2 says, the covariance $C(r)$, a second-order characteristic of random sets, can be easily determined by planar or linear sections. This is possible even in the anisotropic case.

Even more is possible: For germ–grain models with spherical grains the pair correlation function of the point process of ball centres can be determined from thick or planar sections. Of course, in this case high quality images of sections are needed and the grains must be spherical

in very good approximation. Furthermore, pair correlation functions can be estimated from planar sections in the case of fibre processes as well. These methods yield at least qualitative information that may be of value for model building.

10.7.2 Stereological determination of the pair correlation function of a system of ball centres

Let Φ_V be a motion-invariant point process of balls centres with pair correlation function $g_V(r)$. Taking a thick section of thickness t, parallel to the (x_1, x_2)-plane, and projecting onto the (x_1, x_2)-plane give the planar point process Φ_A of the centres of projected section discs. (If $t = 0$, then the thick section becomes a planar section.) Let Φ_A have pair correlation function $g_A(r)$. The function $g_A(r)$ can be estimated statistically using the methods of Section 4.7.4. Under some simplifying assumptions on the diameter distribution, $g_A(r)$ can be related to $g_V(r)$ by a stereological integral equation.

One example is that if the ball diameters are constant, equal to d_V, then

$$g_A(r) = \frac{2}{(d_V + t)^2} \int_0^{d_V+t} (d_V + t - x)\, g_V(\sqrt{r^2 + x^2})\, \mathrm{d}x \qquad \text{for } r \geq 0. \tag{10.83}$$

Figure 10.6 shows $g_A(r)$ for a random dense packing of identical balls, obtained by simulation and statistical estimation based on 2683 section discs. The graph of $g_A(r)$, for the smaller r, looks like that of the pair correlation function of a planar point process with a soft-core behaviour, but for the larger r it is quite similar to the pair correlation function $g(r)$ for the ball centres shown in Figure 4.7 on p. 142. Note that indeed in a planar section, inter-point distances smaller than the ball diameter are possible for the section disc centres.

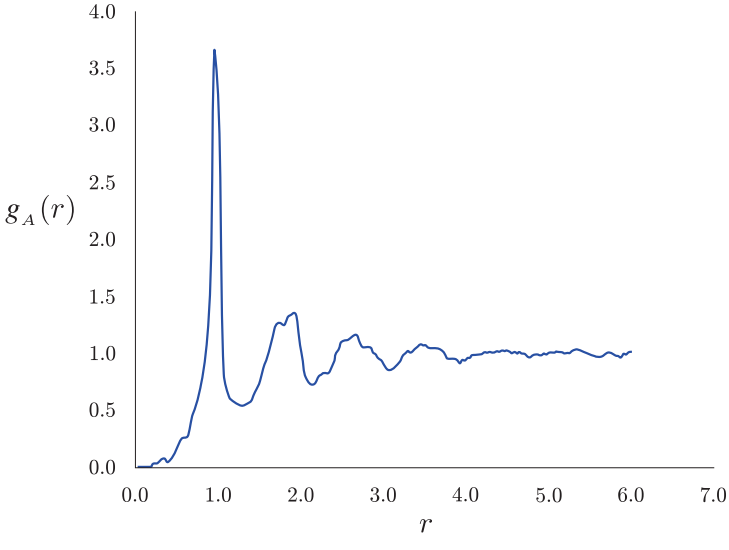

Figure 10.6 Pair correlation function $g_A(r)$ for a system of identical hard balls in $\mathbb{R}^3$. The function was determined statistically from a simulation of the hard ball system with the force-biased algorithm, see Section 6.5.3, based on 2683 section discs in a square window.

If the balls have independent random diameters with distribution function $D_V(r)$ and if individual section discs, even in case of overlapping, can be identified, then $g_A(r)$ and $g_V(r)$ are related by

$$g_A(r) = \int_0^\infty f_V(x,t) g_V(\sqrt{x^2+r^2})\,\mathrm{d}x \qquad \text{for } r \geq 0, \tag{10.84}$$

where

$$f_V(x,t) = \frac{2}{(d_V+t)^2} \int_x^\infty \big(1 - D_V([\|2x-u\|-t]^+)\big)\big(1 - D_V([u-t]^+)\big)\,\mathrm{d}u \quad \text{for } x \geq 0, \tag{10.85}$$

see Hanisch (1983), where $[x]^+ = \max\{x, 0\}$. Formula (10.84) was already given for the special case $t = 0$ of planar sections in Hanisch and Stoyan (1980).

A very simple but rough nonstereological approximation is

$$g_V(r) \approx g_A(r). \tag{10.86}$$

In fact, this is exact in the case of a Poisson process, and in general it is not bad for medium and large r; compare, for example, Figures 10.6 and 4.7. Note also that the covariances satisfy

$$C_A(r) = C_V(r), \tag{10.87}$$

and that Formula (6.100) holds.

Difficulties arise with the above formulae in general because $D_V(r)$ and d_V are unknown and, as seen in Section 10.4, their determination is not easy. However, there is a helpful recommendation for the integral equation (10.88), found by Hanisch (1984a), which expresses $g_V(r)$ in terms of quantities that can be estimated directly from planar sections.

Remark on the proof of Formula (10.83)

The second-order factorial moment measure $\alpha_A^{(2)}$ of Φ_A can be expressed in terms of that of Φ_V, denoted by $\alpha_V^{(2)}$, by

$$\begin{aligned}\alpha_A^{(2)}(B_1 \times B_2) &= \alpha_V^{(2)}(B_1 \times [-\Delta, \Delta] \times B_2 \times [-\Delta, \Delta]) \\ &= \int_{B_1}\int_{-\Delta}^{\Delta}\int_{B_2}\int_{-\Delta}^{\Delta} \alpha_V^{(2)}\,\mathrm{d}\big((x_1,x_2,x_3),(y_1,y_2,y_3)\big),\end{aligned}$$

where $\Delta = (d_V + t)/2$ and B_1 and B_2 are both planar Borel sets. This equation holds because all points of Φ_A in B_1 and B_2 result from points of Φ_V in $B_1 \times [-\Delta, \Delta]$ and $B_2 \times [-\Delta, \Delta]$, and is true for all planar Borel sets B_1 and B_2. The pair correlation functions are densities of the corresponding second-order factorial moment measures (up to constant factors $N_A^2 = N_V^2(d_V+t)^2$ and N_V^2). Therefore a similar equation holds for the pair correlation functions,

$$g_A(r) = \frac{1}{(d_V+t)^2} \int_{-\Delta}^{\Delta}\int_{-\Delta}^{\Delta} g_V\big(\sqrt{r^2+(x_3-y_3)^2}\big)\,\mathrm{d}x_3\,\mathrm{d}y_3. \tag{10.88}$$

This relationship can be transformed into (10.83). The proofs of the other formulae are similar. □

In the case of Formula (10.83) there exists a theoretical solution, $g_V(r)$ can be obtained if $g_A(r)$ is given, as shown by Kalmykov and Shepilov (2000).

If there is an r_1 (the smallest one) such that $g_V(r) = 1$ for $r \geq r_1$, the solution is

$$g_V(r) = \frac{g^*(r)}{\pi} - \frac{d_V}{\pi r}\int_r^{r_1} \frac{x g^{*'}(x)}{\sqrt{x^2 - r^2}}\,\mathrm{d}x + \frac{1}{\pi}\int_r^{r_1} g^*(x) \times \left(\frac{2x}{\pi d_V^2}\exp\left(\frac{x^2 - r^2}{\pi d_V^2}\right)\left(1 + \operatorname{erf}\left(\sqrt{\frac{x^2 - r^2}{\pi d_V^2}}\right)\right) + \frac{2x}{\pi d_V\sqrt{x^2 - r^2}} - \frac{d_V}{(x + r)\sqrt{x^2 - r^2}}\right)\mathrm{d}x \qquad \text{for } \sqrt{r_1^2 - d_V^2} \leq r \leq r_1, \tag{10.89}$$

where

$$g^*(r) = g_A(r) - 1 - \frac{r_1^2 - r^2}{d_V^2} + \frac{2}{d_V}\sqrt{r_1^2 - r^2},$$

and $\operatorname{erf}(x)$ is the error function, which is related to the complementary error function in (9.118) on p. 385 by

$$\operatorname{erf}(x) + \operatorname{erfc}(x) = 1.$$

Shepilov *et al.* (2006) consider an example from glass research. The starting point is a sample of electron microscopic images, representing planar sections. The authors show ordering effects in the arrangement of particles in phase-separated sodium borosilicate glasses.

As with the other integral equations of stereology, (10.83) and (10.84) are difficult to solve numerically, and the solution formula (10.89) is only of limited value, since usually only estimates are known for $g_A(r)$. It may be useful to consult Hanisch (1984a), where $g_A(r)$ is calculated for some spatial models with known $g_V(r)$. Also here a two-step method can be recommended, where in the first step the form of $g_V(r)$ is explored and in the second the corresponding parameters are estimated, using (10.84).

Example 10.5. *Sinter metal balls (Hanisch, 1984a)*
Figure 10.7(a) shows a planar section through a specimen of sinter metal, and Figure 10.7(b) displays the corresponding estimated pair correlation function $g_A(r)$ of the point process of section disc centres. Hanisch assumed that the ball diameters were constant at 1.4; an assumption supported by (10.45) and the measurements for mean and standard deviation of diameters of section discs,

$$\bar{x} = 0.99 \qquad \text{and} \qquad s = 0.32.$$

Numerical solution of the integral equation (10.83) yielded the graph of $g_V(r)$ displayed in Figure 10.7(b).

The differences between $g_A(r)$ and $g_V(r)$ are typical for the case of independent (constant) diameters: the hard-core distance corresponding to g_V is larger than that for $g_A(r)$ while the peaks of $g_V(r)$ are higher and appear at larger values of r. Comparison of $g_V(r)$ with Figure 4.7 on p. 142 suggests the possibility that the balls in the probe form a random dense packing.

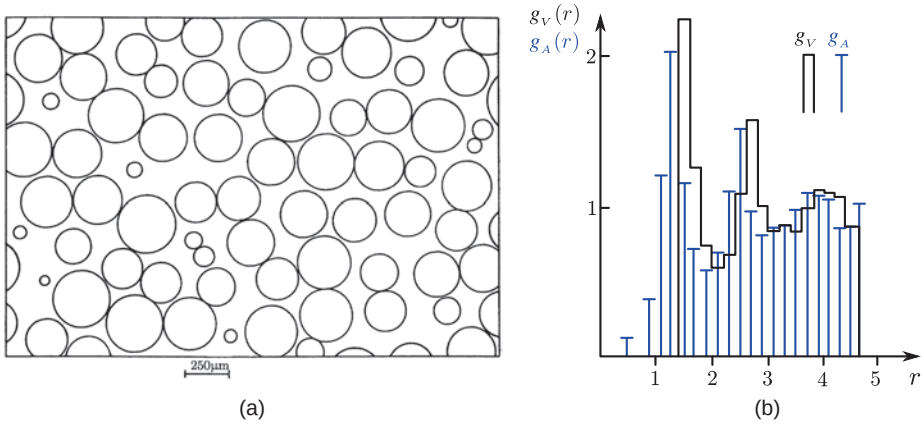

Figure 10.7 (a) Planar section through a specimen of sinter metal. The length unit is approximately 250 μm. (b) The pair correlation functions $g_A(r)$ and $g_V(r)$ for the sinter metal probe. The form of $g_V(r)$ suggests the assumption that the balls form a random dense packing; compare with Figures 4.7 and 10.6.

If the diameters are dependent (as in random dense packings with different ball diameters or in the Stienen model) then different things may happen. This case is studied in a general second-order theory for ball systems given by stationary and isotropic marked point processes as on p. 428; see Stoyan *et al.* (1990). There appears an integral equation which generalises (10.40), involving the planar and spatial pair correlation functions and the family of so-called two-point mark distributions $\mathscr{D}_{V,r}$, which are the joint distributions of the diameters of two balls with given inter-centre distance r under the condition that at two given points of distance r there are ball centres. Stoyan (1990a) uses this integral equation to calculate the pair correlation function $g_A(r)$ of the point process of section disc centres corresponding to the Stienen model; see Figure 10.8, which also contains pair correlation function graphs for the generalised Stienen model, where all diameters are multiplied by a constant factor $\alpha < 1$. (This produces a further system of non-overlapping balls in space, but now without contact between balls and with volume fraction less than 0.125.)

A statistician who is familiar with pair correlation function statistics as described in Illian *et al.* (2008) would classify the pair correlation functions $g_A(r)$ shown in Figures 10.7(b) and 10.8 as pair correlation functions of point processes with a weak form of short-range order of the inhibition type. And indeed, there is a form of inhibition: a point pair of very close section disc centres is only possible if the corresponding balls have a rather extraordinary position. This may explain the form of $g_A(r)$. But of course, the pair correlation function $g_V(r)$ of the Stienen model ball centres is that of a Poisson process and in this case $g_V(r) \equiv 1$. Thus $g_A(r)$ reflects weak inner order of the Stienen model, where the diameters are not independent.

10.7.3 Second-order analysis for spatial fibre systems

Stoyan (1984b, 1985a,b) suggested approximate stereological methods for the determination of the pair correlation function for spatial fibre systems. The method applies both to planar and to thick sections. Under the simplifying assumption that one can ignore the spatial correlations

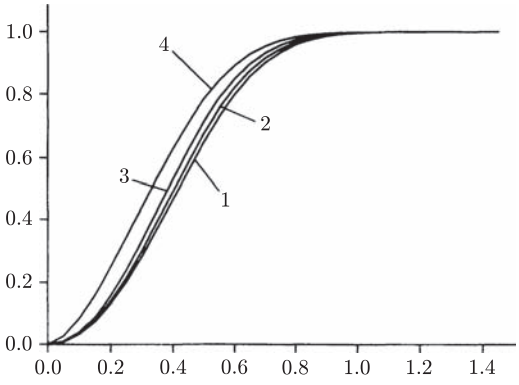

Figure 10.8 The pair correlation function of the point process of section disc centres of the Stienen model with intensity $\lambda = N_V = 1$. Furthermore, the pair correlation functions for generalised Stienen models with $\alpha < 1$ are shown. See text for explanation. ($1 : \alpha = 0.25$, $2 : \alpha = 0.5$, $3 : \alpha = 0.7$, $4 : \alpha = 1$.)

of fibre directions at the fibre section points, an integral equation similar to (10.83) can be derived for the case of thick sections. It connects the pair correlation functions $g_V(r)$ and $g_A(r)$ of the spatial and the projected fibre processes. Figure 10.9(a) shows a thick section of a spatial fibre system, representing a network of dislocation lines induced by diffusion in a

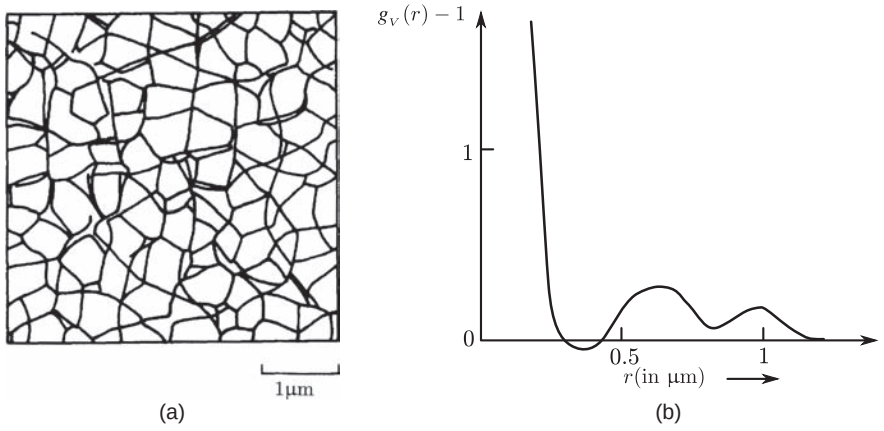

Figure 10.9 (a) Network of dislocation lines induced by diffusion in a silicon crystal, taken from a photograph of a transmission electromicroscopic image in Hanisch *et al.* (1985). The thickness of the foil was about 0.2μm. (b) Estimated spatial pair correlation function $g_V(r)$ of the dislocation lines. The limiting value $g_V(0+)$ is $+\infty$. This is typical for fibre processes as discussed in Section 8.3.1 for the planar case.

single silicon crystal. Figure 10.9(b) gives the corresponding spatial pair correlation function; see Hanisch *et al.* (1985).

Further simplification, as described in Krasnoperov and Stoyan (2006), leads in the case of planar sections to the simple approximation

$$g_V(r) \approx g_A(r), \tag{10.90}$$

where $g_A(r)$ is the pair correlation function of the planar point process of fibre section points, which in applications are usually the centres of section profiles of thick fibres. (Recall that the same approximation has been suggested in (10.86) for systems of ball centres.) Krasnoperov and Stoyan (2006) apply these ideas to the case of blood capillaries.

The case of straight fibres makes some difficulties in all second-order stereological approaches; in Stoyan's papers it is usually excluded or handled in a particular way. Two simple models are the spatial Poisson line process and the Boolean model with segments as grains. In both cases the section with a plane yields a Poisson point process, and thus the pair correlation function $g_A(r)$ does not give interesting spatial information: it is

$$g_A(r) \equiv 1.$$

However, such fibre processes will hardly ever appear in practical applications. They could be called fibre processes 'without structure', since their only spatial correlation comes from the inner connectedness of the segments or lines; between different segments or lines there are no correlations, and each object produces at most only one point of intersection with the section plane.

The following discusses the quality of the approximation (10.90) for a simple fibre process model 'with structure'.

Example 10.6. *The Boolean circle model*
Consider a Boolean model, with germ intensity λ_V. The grains are fibres, closed circular lines of constant radius R of random uniform orientation. Thus the grains are not convex. The union of all circles is the fibre process of interest. Its fibre density is $L_V = 2\pi R\lambda_V$ and the pair correlation function is

$$g_V(r) = 1 + \begin{cases} \dfrac{1}{\pi r^2 L_V}\,\dfrac{R}{\sqrt{4R^2 - r^2}} & \text{for } r \le 2R, \\ 0 & \text{otherwise.} \end{cases}$$

This can be proved as Formula (8.27) in Example 8.4; see also Stoyan and Stoyan (1986).

A planar section produces a Poisson cluster process, where each cluster consists of exactly two points, which belong to the same intersected circle. The intensity of the Poisson process of parent points is $\lambda_A = \pi R^2\lambda_V/2$, using Formula (3.66). Thus the intensity of the point process of all fibre section points is $P_A = \pi R^2\lambda_V$. Its pair correlation function is

$$g_A(r) = 1 + \begin{cases} \dfrac{1}{2\pi r P_A}\,\dfrac{r}{2R\sqrt{4R^2 - r^2}} & \text{for } r \le 2R, \\ 0 & \text{otherwise.} \end{cases}$$

This example shows what the approximation (10.90) can yield: (a) $g_A(r)$ usually does not have a pole at $r = 0$, whilst $g_V(r)$ always has, but (b) other structural properties are indicated in a qualitatively correct form. In the given example $g_V(r)$ as well as $g_A(r)$ have a pole at $r = 2R$, which is related to the circle diameter.

10.7.4 Determination of directional distributions

Stereological problems increase in complexity when the structures under investigation are anisotropic. Anisotropy occurs, for example, for capillaries in skeletal muscles or for grains in rolled steel. In such cases it is common to make sections of different orientations, generally in transverse and longitudinal directions to the main axis of anisotropy if this is known. If the structure can be interpreted as a 'pressed' structure, then formulae as on p. 324 may be employed.

In this section a brief discussion will be given of the case of directional distributions of anisotropic fibre systems; similar considerations for surface systems can be found in Weibel (1980) and Beneš and Rataj (2004).

Several authors suggest parametric approaches; see Weibel (1980), Mathieu *et al.* (1983), Mattfeldt and Mall (1984), Cruz-Orive *et al.* (1985), Jensen *et al.* (1985) and Poole *et al.* (1992). Each fibre direction corresponds to a direction on a hemisphere (or more properly the projective plane) which allows the use of standard distributions on the hemisphere as considered in the theory of directional data; see Fisher *et al.* (1987). In particular the *Fisher* or the *Watson* distribution (Fisher *et al.*, 1987, pp. 86 and 89) may be employed. The latter depends on a concentration parameter κ and this can be determined together with the intensity L_V by using a nonlinear regression procedure. The procedure uses as data the mean number of intersection points of fibres per unit area in planes of various known directions. This approach also enables tests of the goodness-of-fit of the distributional assumption. Given κ it is sufficient to consider just one plane of intersection. Cruz-Orive *et al.* (1985) applied the method to an example concerning the study of orientations of capillaries in the skeletal muscle of cats.

Commencing from the observation that fibres are often tubes, a nonparametric method has been developed; see Stoyan (1984b, 1985b) and also papers on the stereology of tubes such as Baddeley and Averback (1983). If the fibres are of circular cross-section with slowly varying diameter, the angles at which the fibres intersect the plane may be determined by observation of the intersection figures in planar or thick sections. Figure 10.10 illustrates this point.

Figure 10.10 shows that the intersection angle β is given by

$$\cos\beta = \frac{bl + t/\sqrt{l^2 + t^2 - b^2}}{l^2 + t^2}. \tag{10.91}$$

It is possible to measure β automatically by exploiting this formula. An alternative means of measuring β uses the possibility of moving the focal plane up and down when observing thick sections of biological tissue by microscope. The line density L_V can be estimated by

$$L_V = \sum_{i=1}^{n} \frac{1}{\nu_2(W)\cos\beta_i}, \tag{10.92}$$

where β_i is the angle corresponding to the i^{th} intersection figure, and n is the number of intersection figures in the window of observation W.

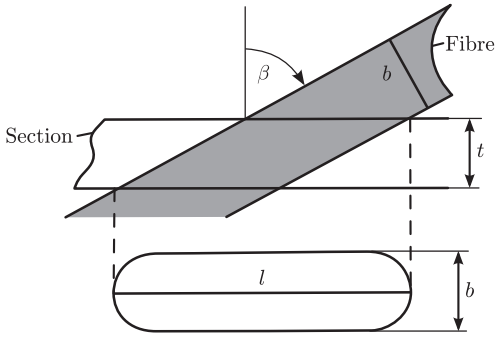

Figure 10.10 Intersection figure for a cylindrical fibre in a thick section. The same figure would occur if the intersection angle was still β and the orientation of the fibre was reversed (so that it would come from left above to right below).

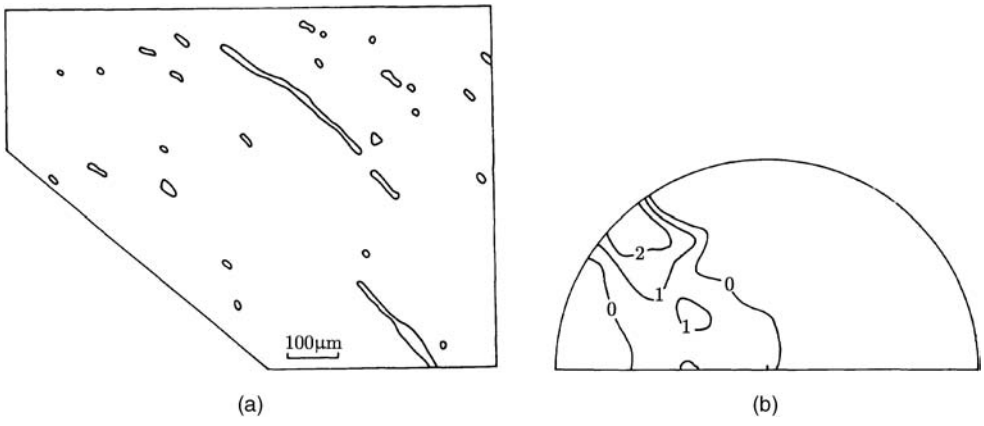

Figure 10.11 (a) Intersections of capillaries with a section from the medullary zone of the human brain, and (b) the corresponding directional distribution, using Schmidt's net representation; the density is given up to a factor of proportionality by contour lines.

Stoyan (1985b) demonstrates how the directional distribution can be determined. Figure 10.11(b) shows the directional distribution, displayed in Schmidt's net, for the specimen of capillaries in the medullary zone of the human brain in Figure 10.11(a) (a description of Schmidt's net can be found in for example Fisher *et al.*, 1987, p. 38). The intersection figures only give fibre directions up to reflection in the normal to the plane of intersection (see Figure 10.10) and so only a half-circle is used.

Beneš and Rataj (2004, section 5.3) discuss a convex-geometry approach.